Collisional-radiative modeling in flow simulations

Marco Panesi
von Karman Institute for Fluid Dynamics
Chaussée de Waterloo 72
1640 Rhode-Saint-Genèse, Belgium
email : panesi@vki.ac.be

Thierry Magin
Center for Turbulence Research
Stanford University, 488 Escondido Mall
Stanford CA-94305, USA
email : magin@stanford.edu

Anne Bourdon
Laboratoire EM2C UPR 288 CNRS
Ecole Centrale Paris, Grande voie des vignes
92295 Châtenay-Malabry Cedex, France
email : anne.bourdon@em2c.ecp.fr

Arnaud Bultel
UMR CNRS 6614 CORIA
Université de Rouen - Site universitaire du Madrillet - BP12
76801 Saint-Etienne du Rouvray cedex, France
email : arnaud.bultel@coria.fr

Olivier Chazot
von Karman Institute for Fluid Dynamics
Chaussée de Waterloo 72
1640 Rhode-Saint-Genèse, Belgium
email : chazot@vki.ac.be

Yacine Babou
von Karman Institute for Fluid Dynamics
Chaussée de Waterloo 72
1640 Rhode-Saint-Genèse, Belgium
email : babou@vki.ac.be

September 8, 2008

Contents

Abstract

The present notes address the modeling of high speed re-entry plasma flows under strong nonequilibrium conditions.
At high re-entry speeds, a significant portion of the heating experienced by the spacecraft can be due to radiation and it is highly influenced by the shape of the internal energy distribution function. In this notes, we propose a kinetic mechanism for air plasma under nonequilibrium conditions. We first analyze the behavior of the electronically excited state of the atoms in the post shock region during an high speed re-entry. The flight conditions are taken from FIRE II flight experiment and from the test conditions in the EAST shock tube facility.
We move then to a more sophisticated model which accounts for non-boltzmann effects for electronic levels of atoms and molecules. Departure of the electronic energy level populations from Boltzmann distributions is found due to depletion of the high lying bound electronic states in the rapidly ionizing regime behind the strong shock wave.

Part I
Atoms

1 Collisional Radiative model: atoms

In this work, we propose to study FIRE II (16), a reentry flight experiment carried out in 1960s. One of the primary objectives of the Fire Project was to estimate the heating that a capsule experiences at high speed conditions ($\geq$ 10 km/s). The focus of this project was the estimation of the radiative component of the heat-flux by measuring directly the incident radiation using on-board radiometers. Moreover, the data collected from the experiment can be used for the validation of flow solver and physical models(47; 37; 49).
In the analysis that follows, we focus our attention on three different points in the trajectory: 1634 s, 1636 s, and 1643 s (elapsed time from the launch). The first two points chosen belong to the earlier part of the trajectory where the flow exhibits strong nonequilibrium effects, whereas for the last point under consideration, the gas is close to equilibrium conditions.
The investigation is carried out by means of a hybrid model that combines the use of an electronic state-to-state CR model for the electronic levels of the atoms and describes the thermal nonequilibrium effects of the other energy modes by means of a multitemperature model. The choice of the atoms is justified by the fact that, for the high temperatures reached at high speeds ($\geq$ 10 km/s), the contribution to the radiative component of the heat flux is dominated by atomic lines and continuum radiation (37; 6; 36), the molecules being almost completely dissociated in this temperature range.
The rates of the electronic-specific reactions are based on the data of the electronic state-to-state CR model recently developed by Bultel et al. (11). A complementary set of reaction rates is taken from Park et al. (56). In this work, the time-dependent CR model is directly coupled with a one-dimensional flow solver to simulate shock-tube experiments. Then, conservation equations of mass, momentum, global energy, vibrational energy, and free-electron energy are solved simultaneously.
The large number of elementary processes considered in the model will allow for a better understanding of the kinetic mechanisms for air plasmas, enabling us to better reproduce the gas kinetics in the shock layer and also describe the electronic energy level populations used to es-

timate radiative heat-fluxes. Furthermore, as the state-to-state CR model is directly coupled to the flow solver, a thorough analysis of the validity of the QSS assumption is also carried out. The physical model is presented in section 1.1, with a description of the CR part and the multitemperature part of the model. Section 2.3 is devoted to simulations of shock-tube flows representative of the Fire II flight experiment. A comparison with results from literature (34; 37) is performed. Then, validity of the QSS assumption is discussed, comparing three different formulations with the fully coupled approach described in section 1.1.

1.1 Physico-chemical modeling

The air mixture used in this work comprises 95 species including the electronic energy levels of atomic nitrogen and oxygen. The vibrational energy level populations of the N_2, O_2, and NO molecules are assumed to follow Boltzmann distributions at the vibrational temperatures T_{vN_2}, T_{vO_2}, and T_{vNO}, respectively; the vibrational populations of the other molecules are associated with the vibration of the N_2 molecule. The rotational energy level populations are assumed to follow Boltzmann distributions at the translational temperature T of the gas. The CR model yields the electronic state populations of the N and O atoms. Thus, their electronic temperature does not need to be specified. The electronic energy populations of the other species are assumed to follow Boltzmann distributions at the translational temperature T_e of the free electrons.

1.1.1 Air mixture

In this study, air is considered as a mixture of nitrogen and oxygen and their products composed of

- Neutral species: N_2, O_2, NO, N(1 − 46), and O(1 − 40),
- Charged species: N_2^+, O_2^+, NO^+, N^+, O^+, and e^-.

Forty-six electronic energy levels for N and forty levels for O are accounted for in Table 1. They allow to accurately calculate: 1) Ionization of the N and O atoms by electron impact; 2) The net population of the metastable states N(2) =N($^2D^0$), N(3) =N($^2P^0$), O(2) = O(^1D), and O(3) =O(^1S) resulting from electron induced processes. Coupling of the atom electronic energy levels through the different elementary processes considered in the following section allows for explicit determination of their excitation and the radiative signature of the plasma without using any a priori assumption on their populations.

Although the O_2^- and O^- species can also be formed, their contribution to chemistry can be considered to be negligible, as a result of the high temperature level reached behind the shock wave and of the high rate coefficient for detachment processes which follows.

1.1.2 Collisional Radiative model

1.1.3 Atomic elementary processes

The inelastic collisions between the mixture species lead to chemical changes. The N and O atoms are efficiently excited and ionized by electron impact reactions; due to their weak mass, free electrons very easily change occupation of the attached electrons of atoms. Several models exist for the related cross sections and rate coefficients. For excitation and ionization of the first three states of N and O, we have used the rate coefficients reported by Bultel et al. (11). Their collisional radiative model for air has been previously used for weaker shock conditions (speeds of 5-6 km/s).

The cross sections proposed by Drawin proved to be efficient in similar conditions (25; 24), and are thus adopted here for excitation and ionization of the higher states. We have expressed the rate coefficients under an analytical form derived from integration of these cross sections over a Boltzmann distribution at the electron T_e. For an electronic transition from the i to j level, where $j > i$, the rate coefficient $k_{i\to j}$ is a function of the secondary quantum number l of each level involved

- For an optically allowed transition ($l_i \neq l_j$):

$$k_{i\to j} = 4\,\pi\,v_e\,a_0^2\,\alpha\,\left(\frac{E_H}{k_B\,T_e}\right)^2\,I_1(a), \tag{1}$$

  where quantity $v_e = [8\,R\,T_e/(\pi M_e)]^{1/2}$ is the electron thermal speed; R, the universal gas constant; M_e, the electron molar mass; $a_0 = 0.529 \times 10^{-10}\,\mathrm{m}$, the first Bohr radius; $E_H = 13.6\,\mathrm{eV}$, the ionization energy of the hydrogen atom; $\alpha = 0.05$; and $I_1(a) = 0.63255\,a^{-1.6454}\,\exp(-a)$, with the reduced energy $a = (E_j - E_i)/(k_B T_e)$.

- For an optically forbidden transition ($l_i = l_j$):

$$k_{i\to j} = 4\,\pi\,v_e\,a_0^2\,\alpha\,\left(\frac{E_j - E_i}{k_B\,T_e}\right)^2\,I_2(a)$$

  with the same notations and where quantity $I_2(a) = 0.23933\,a^{-1.4933}\,\exp(-a)$.

The reverse processes are based on the microreversibility principle, the reverse rate is calculated from the equilibrium constant $K_{eq}(T_e) = (g_j/g_i)\exp(-a)$.
For ionization of an atom under electron impact, Eq. (1) is used with $\alpha = 1$ and a reduced energy $a = (E_i^{ion} - E_i)/(k_B T_e)$, where E_i^{ion} is the energy of the ground state of the ion related to that of the ground state of the atom.

1.1.4 Molecular elementary processes

The kinetic mechanism comprises:

- Dissociation of N_2, O_2, and NO by atomic or molecular impact / recombination,
- Dissociation of N_2 by electron impact / recombination,
- Associative ionization / dissociative recombination,
- Radical reactions (including Zel'dovich reactions),
- Charge exchange.

For direct dissociation by molecular impact, the rate coefficients of Park et al. (56) are computed at the average temperature $(T\,T_{vi})^{1/2}$, where symbol i stands for the index of the molecule being dissociated. The reverse rates are computed at the gas temperature T based on the equilibrium constant. The rate of the nitrogen dissociation reaction by electron impact and of the reverse process is computed at the electron temperature T_e based on the same reference.
Zel'dovitch reactions are known to greatly influence the distribution of nitrogen and oxygen between atomic and molecular systems and contribute to the destruction of O_2 and N_2 and the formation of NO. We have used the rate coefficients obtained by Bose and Candler (4; 5) using a quasi classical trajectory method performed starting from an ab initio potential surfaces

calculation.
The dissociative recombination of the molecular ions is known to play a important role in the case of recombining plasmas (Guberman; 12). In addition, the inverse process, associative ionization, allows for formation of the first electrons in many cases, such as in shock-tubes and reentry problems, and consequently, explains many ionizing situations. In our case, since N_2^+, O_2^+, NO^+ are present in the plasma described here, dissociative recombination has to be considered.

We have have extracted the rate coefficients compiled by Teulet et al. (69), Capitelli et al. (15) and Kossyi et al.(39) those related to charge transfer (with possible reassociation of atoms to form a molecule), reassociation, excitation transfer, ionization, and dissociation. Due to the pressure levels involved in our CR model, we have also taken into account the previous processes occurring when a third particle interacts. For further details, refer to (11).

1.1.5 Radiative processes

At speeds higher than 10 km/s, the radiative signature of heated N_2 and O_2 mixtures is mainly due to the spontaneous emission of the N and O atoms. Since our atomic model is based on grouping elementary levels having similar characteristics, the equivalent spontaneous emission probability of each level has to be determined. Related data taken from the NIST (National Institute of Standards and Technology) database (45) are given in Table 2). In total, we take into account 45 spontaneous emission lines for N and 24 lines for O. The possible re-absorption of radiation is estimated making use of an escape factor α. In the following analysis, we assume that an optically thin medium is described by a value of $\alpha = 1$, whereas for an optically thick medium $\alpha = 0$.

1.1.6 Shock-Tube flow solver

We have developed a one-dimensional flow solver, SHOCKING, to simulate air plasmas obtained in shock-tube facilities, based on the model presented in (44). This model has been modified to simulate reentries at speeds higher than 10 km/s. First, a radiative source term Q_{Rad} has been added in the equation that expresses conservation of the total energy. Indeed, radiative transitions tend to deplete the flow energy for an optical thin medium. Second, a separate equation for the energy of the free electrons has been considered since the flow is significantly ionized.

1.1.7 Conservation equations

Post-shock conditions are derived from jump relations assuming frozen gas composition and vibrational and electronic energy modes, the rotational mode being in equilibrium with the translational mode. Then, the downstream flowfield is found by solving conservation equations of mass, momentum, global energy, vibrational energy of the N_2, O_2, and NO molecules, respectively, and a separate energy equation for the free electrons and species with electronic energy

level populations assumed to follow Boltzmann distributions:

$$\frac{\partial}{\partial x}\left(\rho_i u\right) = M_i\,\dot{\omega}_i, \qquad i \in \mathcal{S} \tag{2}$$

$$\frac{\partial}{\partial x}\left(\rho u^2 + p\right) = 0 \tag{3}$$

$$\frac{\partial}{\partial x}\left[\rho u\left(h + \tfrac{1}{2}u^2\right)\right] = -Q^{Rad} \tag{4}$$

$$\frac{\partial}{\partial x}\left(\rho u y_m e_m^V\right) = M_m\,\dot{\omega}_m e_m^V + \Omega_m^{VT} + \Omega_m^{VV} - \Omega_m^{EV}, \qquad m \in \mathcal{V} \tag{5}$$

$$\frac{\partial}{\partial x}[\rho u(y_e e_e + \sum_{i\in\mathcal{E}} y_i e_i^E)] = -p_e\frac{\partial u}{\partial x} + \sum_{i\in\mathcal{E}} M_i\dot{\omega}_i e_i^E - \Omega^I - \Omega^E + \Omega^{ET} + \Omega^{EV} \tag{6}$$

where symbol $\mathcal{S}$ stands for the set of indices of the mixture species, $\mathcal{V}$, the set of indices of the N_2, O_2, and NO molecules, and $\mathcal{E}$, the set of indices of the N^+, O^+, N_2, O_2, NO, N_2^+, O_2^+, and NO^+ species, whose electronic energy populations are assumed to follow Boltzmann distributions. Symbols $\mathcal{N}$ and $\mathcal{O}$ stand for the set of indices of the electronic energy levels of the N and O atoms. Thus, the set of indices of the heavy particles is given by $\mathcal{H} = \mathcal{N} \cup \mathcal{O} \cup \mathcal{E}$ and the set of the mixture species by $\mathcal{S} = \mathcal{H} \cup \{\mathrm{e}\}$. The mass density of species i reads ρ_i, and its molar mass, M_i. The mixture mass density is given by the expression $\rho = \sum_{j\in\mathcal{S}} \rho_j$, the mixture energy, $e = \sum_{j\in\mathcal{S}} y_j e_j$, with the mass fraction $y_i = \rho_i/\rho$, the mixture enthalpy $h = e + p/\rho$, the pressure $p = \rho RT \sum_{j\in\mathcal{H}} (y_j/M_j) + \rho R T_e y_e/M_e$. The species energy e_i, $i \in \mathcal{S}$, comprises the translational and formation contributions $[e_e = e_e^T(T_e) + e_e^F]$ for electrons; the translational, electronic, and formation contributions $[e_i = e_i^T(T) + e_i^E + e_i^F]$ for the electronic energy states N(i), $i \in \mathcal{N}$, and O(i), $i \in \mathcal{O}$; the translational, electronic, and formation contributions $[e_i = e_i^T(T) + e_i^E(T_e) + e_i^F]$ for the N^+ and O^+ ions; and the translational, rotational, vibrational, electronic, and formation contributions $[e_i = e_i^T(T) + e_i^R(T) + e_i^V(T_{vi}) + e_i^E(T_e) + e_i^F]$ for all the molecules, where T_{vi} is the vibrational temperature of the i molecule. The number of electronic levels used to compute the energy of the ions and molecules is tuned to yield the best matching agreement between values of the computed energies and the reference tables of Gurvich et al.(33). Energy of molecules is computed assuming the rigid rotor and harmonic oscillator approximations. Spectroscopic constants are taken from (33). Electronic specific data have been used for the vibrational and rotational constants of the molecules.

1.1.8 Energy relaxation terms

Radiative losses are modeled by means of the Q^{Rad} term in the energy equation. This term represents the radiant power emitted per unit volume and is directly given by the expressions

$$Q^{Rad} = \alpha \sum_{\substack{i,j\in\mathcal{N}\\ j<i}} (E_i - E_j)\,A_{ij}N_i + \alpha \sum_{\substack{i,j\in\mathcal{O}\\ j<i}} (E_i - E_j)\,A_{ij}N_i \tag{7}$$

where A_{ij} is the Einstein coefficient, N_i, the number density of the excited state, and α, the escape factor.

At high speeds, it is important to account for the energy lost by the free electrons during ionization and excitation of the atoms and molecules, as already stressed in (52)-(59). Otherwise, electron impact ionization reactions, and in general all the reactions involving free electrons, produce a large amount of free electrons without depleting their kinetic energy, thus enhancing their production. This phenomenon may lead to an avalanche ionization with consequent related

numerical problems, especially for high speed conditions. Here is an expression for the related source terms for electron-impact ionization and excitation reactions

$$\Omega^I = \sum_{r\in\mathcal{R}^I} \dot{\omega}_{e,r}\mathcal{U}^r, \quad \Omega^E = \sum_{r\in\mathcal{R}^E} \dot{\omega}_{e,r}\mathcal{U}^r \tag{8}$$

where $\mathcal{U}^r$ is the reaction enthalpy of the r reaction, and $\dot{\omega}_{e,r}$, the electron chemical production term of the r reaction. Symbol $\mathcal{R}^I$ denotes the set of indices of the electron-impact ionization reactions, and $\mathcal{R}^E$, the set of indices of electron-impact excitation reactions. The first term Ω^I accounts for the energy removed by electron-impact ionization reactions, and the second term, Ω^E for the energy removal by electron-impact excitation reactions.

The rate of vibrational-translational energy transfer follows a Landau-Teller formula:

$$\Omega_m^{VT} = \rho_m \frac{e_m^V(T) - e_m^V(T_{vm})}{\tau_m^{VT}(T)}, \quad m \in \mathcal{V}. \tag{9}$$

The average relaxation time is given by quantity $\tau_m^{VT} = \sum_{j\in\mathcal{H}}(\rho_j/M_j)/\sum_{j\in\mathcal{H}}[\rho_j/(M_j\tau_{mj}^{VT})]$, where the species relaxation time τ_{mj}^{VT} is based on Millikan-White's formula including Park's correction (52). For the vibrational-vibrational energy exchange, different formulations have been tested. The one proposed by Candler (13) and modified by Knab et al (38) has been chosen:

$$\Omega_m^{VV} = \sum_{l\in\mathcal{V}} \mathcal{N}_A\sigma_{ml}P_{ml}\sqrt{\frac{8RT}{\pi\mu_{ml}}}\frac{\rho_l}{M_l}\rho_m\left(e_m^V(T)\frac{e_l^V(T_{vl})}{e_l^V(T)} - e_m^V(T_{vm})\right) \tag{10}$$

where the exchange probability P_{ml} is assumed to be equal to 10^{-2}, as suggested in (13). Symbol μ_{ml} denotes the reduced molar mass, and $\mathcal{N}_A$, Avogadro's number.

The energy lost by electrons through elastic collisions with heavy particles is written as follows:

$$\Omega^{ET} = \frac{\frac{3}{2}n_e k_B\,(T - T_e)}{\tau_e^{ET}(T_e)}. \tag{11}$$

The relaxation time is obtained from kinetic theory, $1/\tau_e^{ET} = \sum_{j\neq e}(m_e/m_j)\nu_{ej}$, where the collision frequencies read $\nu_{ej} = (8/3)v_e n_j \bar{\Omega}_{ej}^{11}$.

To model the exchange between the vibrational energy and the free-electron energy, we only consider molecular nitrogen, since this molecule is more efficient than O_2 and NO for this kind of process. This rate is assumed to follow a Landau-Teller formula:

$$\Omega^{EV} = \rho_{N_2}\frac{e_{N_2}^V(T_{v_{N_2}}) - e_{N_2}^V(T_e)}{\tau_e^{EV}(T_e)}. \tag{12}$$

The relaxation time taken from (10) is preferred to the analytical form of Lee (42) that overestimates the relaxation time by a factor of 2.3 (10).

Following the derivation of Thivet (70), the conservative system of Eqs. (2)- (6) is transformed into a system of ordinary differential equations easily solved by means of the LSODE (57) library.

1.2 Results: FIRE II

In this section, we apply the collisional radiative model previously described to FIRE II, a well-known flight experiment from the 1960's. One of the primary objectives of the Fire project was to define the radiative heating environment associated with the reentry of a large-scale Apollo vehicle at a velocity of 11.4 km/s. During this reentry, a large portion of the overall wall heat flux was due to radiation. Most of the radiation (approximately 90%) comes from atomic lines (37), thus, an accurate prediction of the populations of excited electronic states of the atoms is crucial. The aim of the present work is to test the CR model for different physico-chemical conditions, from electronic energy level populations in strong nonequilibrium to populations following Boltzmann distributions. Starting from the earliest trajectory points, we move to a description of a point approaching peak heating.

The first part of this section is devoted to thermal nonequilibrium effects in the flow. We study the influence of separating the free electron energy from the vibrational energy and compare our results for temperature and ionization degree with literature data. The rest of the section is devoted to a detailed analysis of the physico-chemical state of the plasma for three trajectory points: 1634 s, 1636 s, and 1643 s elapsed time from the launch. The validity of the QSS assumption often used to compute the excited electronic states is investigated for the 1634 s case by comparing the electronic energy level populations of atomic nitrogen obtained with the QSS assumption to the populations obtained by means of the full CR model.

The set of shock-tube operating conditions corresponding to the three trajectory points investigated here can be found in Table 3. Free stream characteristic quantities are denoted by the subscript $_1$, post-shock characteristic quantities by the subscript $_2$. Symbols u stands for the shock velocity. The mole fractions of nitrogen and oxygen are assumed to be constant through the shock ($x_{\mathrm{N}_2} = 0.79$ and $x_{\mathrm{O}_2} = 0.21$). We recall that, after the shock, the rotational temperature is equal to the post-shock gas temperature T_2, whereas the vibrational and electron temperatures are still equal to the free stream gas temperature T_1.

1.2.1 Analysis of the Fire II 1634 s case

We investigate the physico-chemical state of the plasma corresponding to the 1634 s trajectory point. We show that the flow is characterized by strong thermo-chemical nonequilibrium and depleted populations of the upper electronic energy levels of atoms.

1.2.2 Thermal relaxation

In this section, we estimate the influence of the assumption of thermal equilibrium between the free electron energy/Boltzmann electronic energy and the vibrational energy of N_2 on the results. Two different assumptions are used: 1) Two separate temperatures: $T_{v\mathrm{N}_2}$, for the vibration of N_2 and, T_e, for the translation of the free electrons and electronic excitation of the species following a Boltzmann distribution; 2) One common temperature $T_{v\mathrm{N}_2} = T_e$ for all these energy modes. After the shock, no electrons are present since we have assumed the chemistry to be frozen in the jump relations. Moreover, the electronic populations of molecular nitrogen and oxygen follow Boltzmann distribution at the free stream temperature T_1. Figure 1 shows how thermal nonequilibrium ($T_{V_{\mathrm{N}_2}} \neq T_e$) is restricted to a narrow zone after the shock (≤ 0.4 cm) and has a negligible influence on the evolution of the post shock temperatures and electronic energy populations for atomic nitrogen. The populations of the higher energy levels computed based on $T_{v\mathrm{N}_2} = T_e$ are overestimated in this zone. The thermal nonequilibrium zone is associ-

ated with a small electron number density (see Fig. 2). As soon as the electron density becomes significant, thermal relaxation is very fast, via the efficient EV energy exchange processes[1]. Judging these discrepancies negligible, we have decided to assume that $T_{v\mathrm{N}_2} = T_e$ in the remainder of this work and to solve the following equations

$$\begin{aligned}\frac{\partial}{\partial x}[\rho u(y_{\mathrm{N}_2} e^V_{\mathrm{N}_2} + y_e e_e + \sum_{i\in\mathcal{E}} y_i e^E_i)] &= M_{\mathrm{N}_2}\,\dot{\omega}_{\mathrm{N}_2} e^V_{\mathrm{N}_2} + \Omega^{VT}_{\mathrm{N}_2} + \Omega^{VV}_{\mathrm{N}_2} - p_e\frac{\partial u}{\partial x} + \sum_{i\in\mathcal{E}} M_i\dot{\omega}_i e^E_i \\ &\quad -\Omega^I - \Omega^E + \Omega^{ET} \qquad (13)\\ \frac{\partial}{\partial x}\left(\rho u y_m e^V_m\right) &= M_m\,\dot{\omega}_m e^V_m + \Omega^{VT}_m + \Omega^{VV}_m, \qquad m \in \{\mathrm{O}_2, \mathrm{NO}\} \qquad (14)\end{aligned}$$

instead of Eqs. (5) and (6).

In Fig. 2.1, we compare our four-temperature profiles ($T = T_r$, $T_{v\mathrm{N}_2} = T_e$, $T_{v\mathrm{O}_2}$ $T_{v\mathrm{NO}}$) with the two-temperature profiles ($T = T_r$, $T_v = T_e$) obtained by Johnston (37). While the vibrational free-electron temperature results agree quite well, discrepancies are found in the relaxation of the ro-translational temperature.
Figure 2.2 shows the electron number density for different values of the escape factor α (from 0 to 1) and allows for the influence of the optical thickness on the results to be emphasized. We can appreciate how the free-electron number density rises rapidly after a distance of 0.4 cm due to the electron-impact ionization reactions. In the optically thick case ($\alpha = 0$), the electron population reaches an asymptotic value, whereas in the optically thin case ($\alpha = 1$), the curve exhibits a maximum after which the plasma loses energy and recombines due to radiative cooling.
In the same figure, we have also plotted the electron number density obtained by means of the two-temperature model of Park (56) assuming a Boltzmann distribution among the electronic energy levels. The rate of ionization obtained in this case is higher.

1.2.3 Composition and electronic energy populations

Characterization of the physico-chemical state of the plasma in the shock layer requires the knowledge of the chemical composition, as well as the determination of the energy stored into the internal modes. In Fig. 3, we examine the evolution of the different species concentrations. We recall that only molecular nitrogen and oxygen are present after the shock. These molecules first dissociate, in particular, molecular oxygen tends to completely disappear in favor of atomic oxygen right after the shock, while the full dissociation of molecular nitrogen is delayed. Ionization occurs simultaneously and produces free electrons, nitrogen atom ionization being more efficient than ionization of the other species. Figure 3.2 shows electronic state specific population profiles for atomic nitrogen. It is interesting to mention that the upper electronic states are more reactive than the ground state and lower (metastable) states. Immediately after the shock, the populations of the excited levels tend to equilibrate with the free electron populations that are in nonequilibrium. Moreover, we can observe how the atom populations are mainly in the ground electronic state at the beginning of the relaxation, consistent with the kinetic mechanism assuming that dissociation of molecular nitrogen and oxygen generates atoms in the ground state:

$$\begin{aligned}\mathrm{N}_2 + \mathrm{M} &\rightleftharpoons \mathrm{N}(1) + \mathrm{N}(1) + \mathrm{M}\\ \mathrm{O}_2 + \mathrm{M} &\rightleftharpoons \mathrm{O}(1) + \mathrm{O}(1) + \mathrm{M}\end{aligned}$$

[1]It is worth to notice that thermal nonequilibrium could have been even larger if the relaxation time of Lee had been used instead of the one of Bourdon and Vervisch.

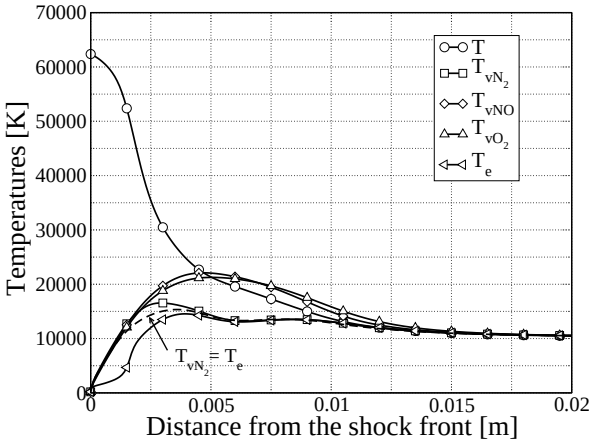

1.1: **Temperature profiles**

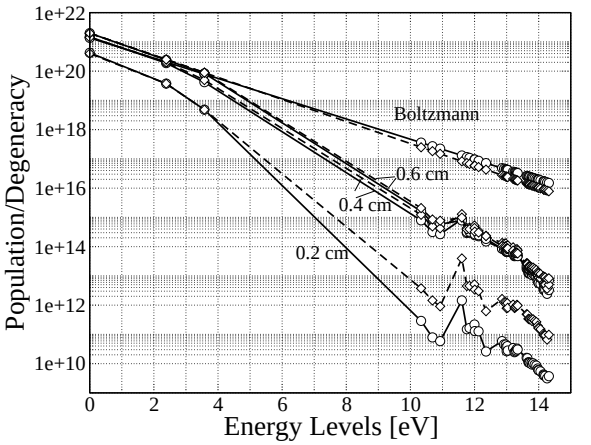

1.2: **Electronic energy level populations for atomic nitrogen $[m^{-3}]$: CR model at 0.2 cm, 0.4 cm, and 0.6 cm; Boltzmann distribution at 0.4 cm.**

Figure 1: 1634 s case. Comparison between the five temperature model with $T_{v\mathrm{N}_2} \neq T_e$ (unbroken line) and the four temperature model with $T_{v\mathrm{N}_2} = T_e$ (dashed line).

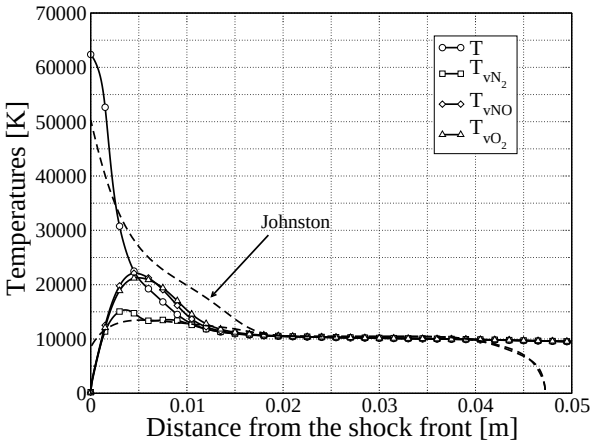

2.1:

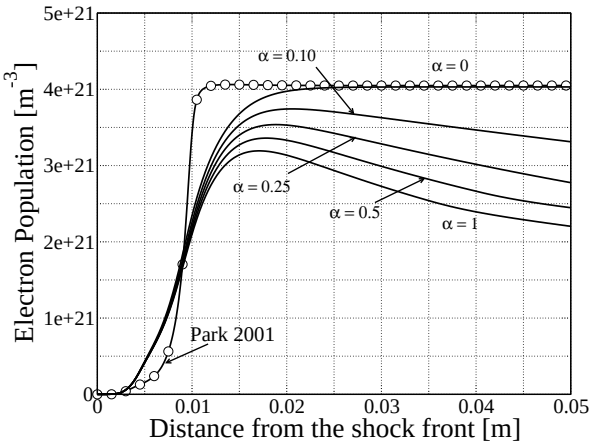

2.2:

Figure 2: 1634 s case. (a) Temperature profiles: CR model (unbroken line); Johnston's results (37) (dashed line). (b) Electron number density profiles: CR model with escape factor values of 0, 0.1, 0.25, 0.5, and 1 (unbroken line); simplified kinetic mechanism of Park et al. (56) (line with circles).

The same assumption holds for all the other reactions (in particular for the Zel'dowich reaction responsible for the atomic nitrogen formation). This assumption is justified since electronic excitation mainly occurs via electron impacts; the number density of electrons is still low in the post-shock region.
After this incubation distance, the number density of electrons significantly increases and the electronic states of atoms thermalize. The electron-impact excitation processes:

$$\mathrm{O(i)} + \mathrm{e^-} \rightleftharpoons \mathrm{O(j)} + \mathrm{e^-}$$
$$\mathrm{N(i)} + \mathrm{e^-} \rightleftharpoons \mathrm{N(j)} + \mathrm{e^-}$$

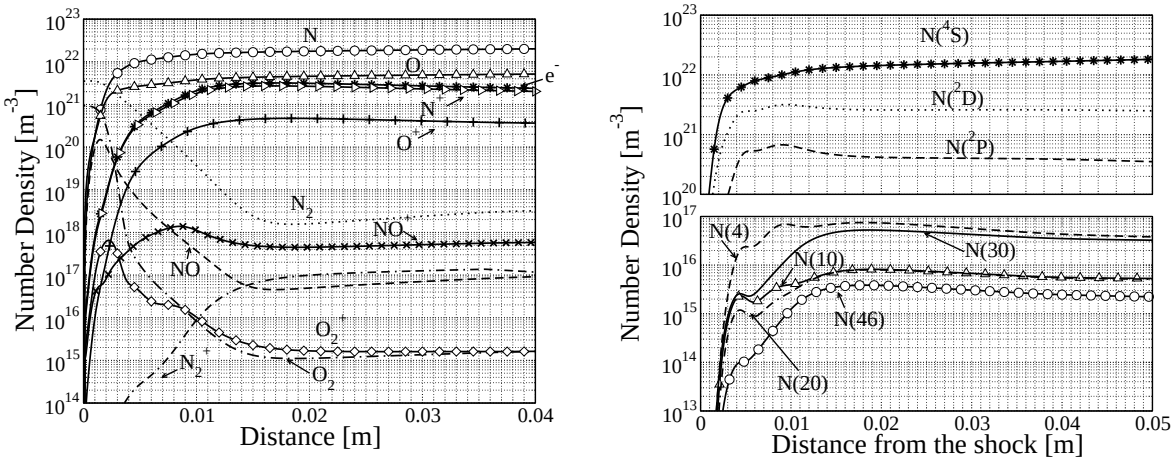

3.1: 3.2:

Figure 3: 1634 s case, number density profiles (a) Mixture species. (b) N(1), N(2), N(3), N(4), N(10), N(20), N(30), N(40).

are fast and the populations of excited electronic states rapidly increase. The upper states are then depleted, in particular by ionization and spontaneous emission, which explains the maximum found in the population profiles.

In order to characterize nonequilibrium of the populations, the number density of the electronic states of atomic nitrogen is compared in Fig. 4 with the Boltzmann and Saha distributions at two locations after the shock. Both Boltzmann and Saha distributions are computed based on the electron temperature T_e by keeping the atomic nitrogen concentration constant. In logarithmic scale, they appear as two parallel straight lines of slope proportional to $-1/T_e$.
In Fig. 4.1, at 0.7 cm from the shock, the CR model predicts that the ground and metastable states follow the Boltzmann distribution, whereas the number density of the highly excited states is much lower and tend to the Saha distribution. This phenomenon is typical of nonequilibrium conditions encountered during high speed reentries. Excellent agreement is found with the results presented in (37).
Figure 4.2 shows the same quantities at 2.5 cm from the shock. Since we have moved at further distance from the shock front, the flow tends towards equilibrium, and the Saha distribution tends to the Boltzmann distribution. Our model predicts that the high lying excited states are still being depleted by radiative exchange with lower states. We notice that at this location the comparison with literature is not as good. Our results show a higher degree of nonequilibrium than in (37), closer to the Boltzmann distribution.

1.2.4 Standard QSS approach

Quasi-steady-state models are often used in the literature (51; 37) to study electronic energy level populations in strong nonequilibrium conditions, under which the hypothesis of a Boltzmann distribution does not hold. They constitute a valid alternative to the time-dependent CR model presented in this paper when the characteristic time of the excited state processes is very short with respect to the characteristic time of the flow. As a consequence, the set of mass conservation equations for the electronically excited states given in Eq. (2) can be expressed as a set of non linear algebraic equations to be solved separately from the other conservation equations. It is important to emphasize that this operation does not reduce the computational cost if the

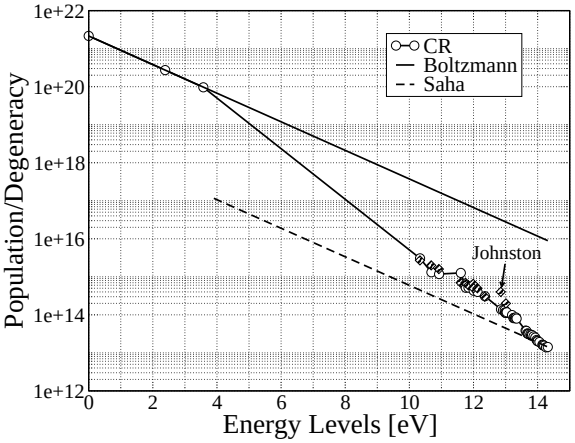

4.1: 0.7 **cm from the shock front.**

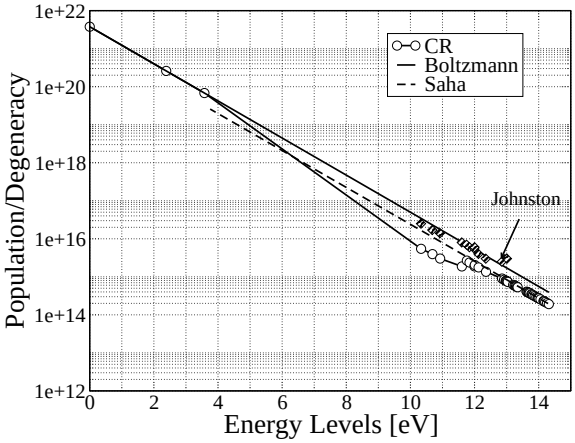

4.2: 2.5 **cm from the shock front.**

Figure 4: 1634 s case. Electronic energy level populations for atomic nitrogen [m^{-3}]: CR model (line with circles), Boltzmann distribution (unbroken line), Saha distribution (dashed line), and Johnston's results (37) (black diamonds)

electronic energy populations are computed everywhere in the flow. The QSS assumption is only desirable when the populations of excited states are probed at some locations of interest, for instance along the stagnation line in multidimensional flow simulations, and therefore, allowing for a drastic reduction of the computational cost versus the time-dependent CR model.
It is well-known that the regime of validity of the QSS assumption is strongly influenced by a sudden change in the plasma conditions, such as after a strong shock where the electron density is very scarce. Since the collisional processes are responsible of the equilibration of the internal energy states, in particular the processes involving electrons as collision partners, a lack of electrons contributes to the failure of the QSS assumption.

In this section, we compare the results obtained by means of the time-dependent CR model to the standard QSS methods presented in (37; 51). First, we compute the profiles of the flow characteristic quantities (pressure, temperatures, and composition) based on the effective reaction rates of Park et al. (56) for air chemistry, widely used in the literature but different from the mechanism given in section 1.1. Then, the QSS populations of excited states are computed at a given location by solving the following system of ordinary differential equations

$$\frac{d}{dt}y_i = \frac{M_i\dot{\omega}_i}{\rho}, \qquad i \in \mathcal{N}_1 \cup \mathcal{O}_1 \tag{15}$$

where the index i runs over all the excited states of N and O, including the metastable states. Our approach, formally different from the system of nonlinear algebraic equations described by the law of mass action, $\dot{\omega}_i = 0$, $i \in \mathcal{N}_1 \cup \mathcal{O}_1$, has an equivalent solution for $t \to \infty$. Our method presents the advantage to overcome numerical problems sometimes encountered when using the algebraic formulation (51; 37). The population of the ground states is retrieved by ensuring that the total number density computed during the flow calculation is conserved in the QSS calculation.

In the following analysis, we examine the first trajectory point at a location of 0.7 cm from the shock front. We compute the electronic energy populations of nitrogen atoms based on three models:

1. Full CR: the time-dependent CR model described in section 1.1,
2. QSS Abba: QSS model with the same data for the atomic and radiative elementary processes as in the full CR model,
3. QSS Park: QSS model with the energy levels and data for the atomic and radiative elementary processes of Park (51).

The main differences between the various models are the coupling method and the sets of data for the reaction rates. For both QSS models, the flow calculations have been performed by clipping the reaction rates of (56) in order to avoid using them out of their validity range; the translational temperature driving the rate constants has been limited to the value of 30 000 K. Moreover, the free-electron energy loss term for electron impact ionization given in Eq. (13) is computed based the expression suggested in (37)

$$\Omega^I = -\omega_{N^+} I^{N^+} - \omega_{O^+} I^{O^+} \tag{16}$$

where $I^{N^+} = 4.05 \times 10^8$ J/(kg mol) and $I^{O^+} = 4.30 \times 10^8$ J/(kg mol), respectively. In the full CR model, we recall that this term is directly computed based on Eq. (8) from the expressions for the reaction rates intrinsic to the model, without any a priori hypothesis.
Figure 5 shows a comparison between the results obtained by means of the three models, the Boltzmann distribution, and Johnston's results. The full CR model and the QSS Abba model yield electronic energy level populations in rather good agreement with Johnston's results. The QSS Abba model slightly underpredicts the population of the lower electronic levels. The QSS assumption is a fair approximation at this location. The differences between the QSS Abba results and the QSS results of Johnston are not well understood, they might be explained by the different data for the electron-impact excitation rates of atoms or for the radiative processes. The differences with respect to the QSS Park model for atomic and radiative processes are significant: up two orders of magnitude for the upper levels above the metastable states.

In conclusion, the standard QSS approach seems to be valid, *at this location*, provided that a correct set of reaction rates is chosen for the model. This choice should be based on a comparison of the computed results with experimental data.
In the flow calculation, the need for a special adjustment for the effective rate constants of Park et al. (56) (maximum temperature) and for the source term responsible for the energy removal from the free electron temperature makes difficult its extrapolation to generic flow conditions.

1.2.5 Towards a simplified CR model

In the foregoing section, we have studied the standard QSS approach by comparing QSS results and time-dependent CR results at one location in the flow. In this comparison, the reaction rate data are not identical, for instance the rates of molecular elementary processes used in the full CR model differ from the rates used in the QSS Abba model. In this section, we further investigate the validity of the QSS assumption, based on the same set of reaction rates, at several locations in the flow. This is a preliminary step to derive a simplified CR model for reentries at speeds higher than 10 km/s, typical of Moon returns.

For this purpose, we compute the electronic energy populations of atomic nitrogen for the first trajectory point (1634 s case) by means of the full CR model. From the calculation, we extract the profiles of the flow characteristic quantities (pressure, temperatures, and composition). Then, the QSS populations of excited electronic states are computed at a given location by

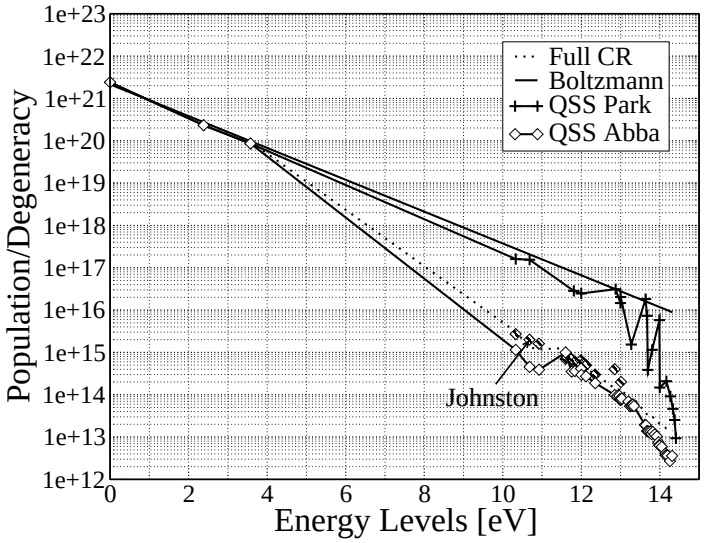

Figure 5: 1634 s case, 0.7 cm from the shock front. Electronic energy level populations for atomic nitrogen [m^{-3}]: full CR model (dotted line), QSS Abba model (line with diamonds), QSS Park et al. model (56) (crosses), Boltzmann distribution (unbroken line), and Johnston's results (37) (black diamonds)

solving the system of Eqs. (15). This approach is called "simplified CR model" in the following. The QSS distribution of excited states is computed by solving the set of Eqs. (15). In the first model (simplified CR metastable) the index runs from $i = 2$ to the total number of electronic levels for the atomic species, whereas in the second model (simplified CR) the metastable states are considered in Boltzmann equilibrium with the ground state and i starts from 4. The latter hypothesis is justified by the small difference in terms of electronic energy among the ground state and the two metastable states which enhances the excitation due to impacts with light and heavy particles promoting thermalization. At the instant $t = 0$ the initial population is assumed to be Boltzmann at the prescribed pressure and temperature conditions[2]. A careful analysis of the system (15), reveals that the population of the ground state and the one of the two metastable states (for the second model, the simplified CR model) is needed in order to close the system of equations. In the first case the population of the ground state is retrieved summing the population of the excited states and subtracting this value to the total number density given by the flowfield calculation.

The flow is investigated at three locations: 0.3 cm, 0.5 cm, and 1 cm from the shock. The electronic energy level populations for atomic nitrogen are shown in Fig. 6. At 0.3 cm, the populations obtained by means of the simplified CR model are higher than the populations obtained by means of the full CR model; the QSS assumption is not valid in the near shock region. This difference of populations is much more pronounced for the metastable states that follow a Boltzmann distribution when the QSS assumption is used. At 0.5 cm, all the excited states practically satisfy the QSS condition. After 1cm, no difference is noticed between the results obtained by means of the two models. An explanation is found by examining the characteristic time for the atomic excitation and ionization processes. For instance, we find that this characteristic time for the first metastable state is of the same order of magnitude as the characteristic time of the flow 5×10^{-6} s computed at 1 cm from the shock.

[2]The initial distribution does not have any influence on the results that depend only on temperature, pressure and the total number of atoms

Based on this analysis, we recommend to keep the atomic metastable states as separate species for this trajectory point and compute the upper electronic states by means of a QSS model, in order to reduce the computational cost in multidimensional flow simulations. The CR model could be used as a tool to derive effective reaction rates for the simplified mechanism associated with this mixture of species and also the expressions for the free-electron energy loss term for electron impact ionization and ionization reactions.

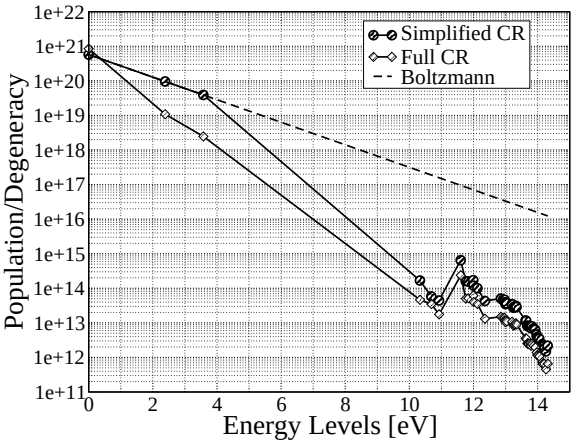

6.1: **0.3 cm from the shock front.**

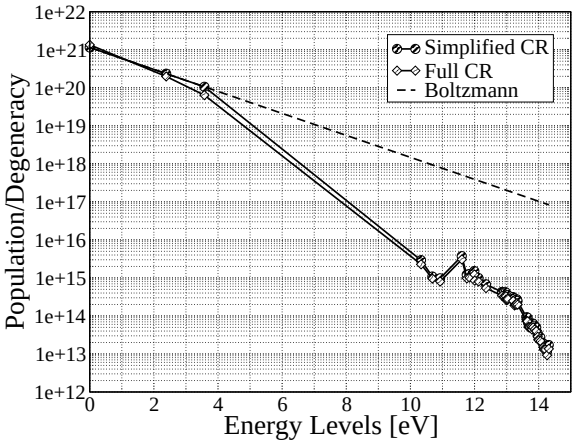

6.2: **0.5 cm from the shock front.**

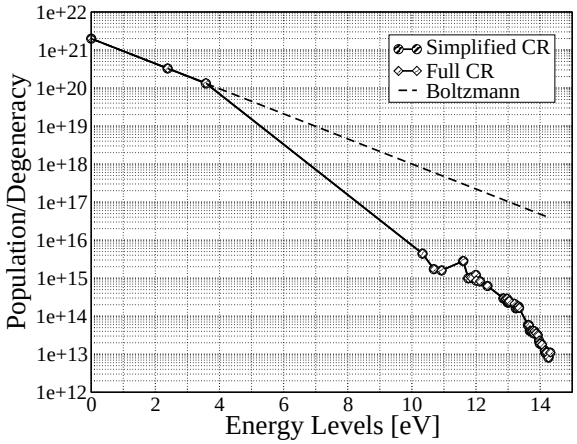

6.3: **1 cm from the shock front.**

Figure 6: 1634 s case. Electronic energy level populations for atomic nitrogen [m^{-3}]: simplified CR model (line with circles), full CR model (line with diamonds), Boltzmann distribution (dashed line).

1.2.6 Analysis of the Fire II 1636 s case

1.2.7 Thermal nonequilibrium effects

In order to demonstrate that the onedimensional flow solver SHOCKING is capable of reproducing the main physico-chemical features along the stagnation line of reentry flows, except for the boundary layer region, we compare our results to simulations obtained by means of validated flow solvers: Laura, DPLR (34) and the viscous shock layer code of Johnston (37). The

comparison is carried out for the temperature and ionization profiles.

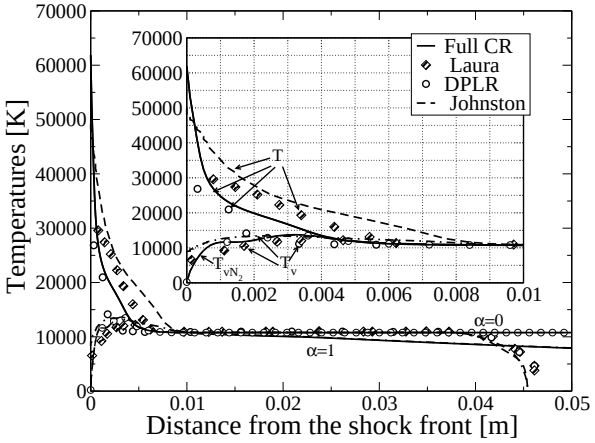

7.1: **Temperature profiles: comparison with results from literature (34)-(37). CR model with escape factor values of 0 and 1 (unbroken line), Laura code (diamonds), DPLR code (34) (circles), and Johnston's results (37) (dashed line).**

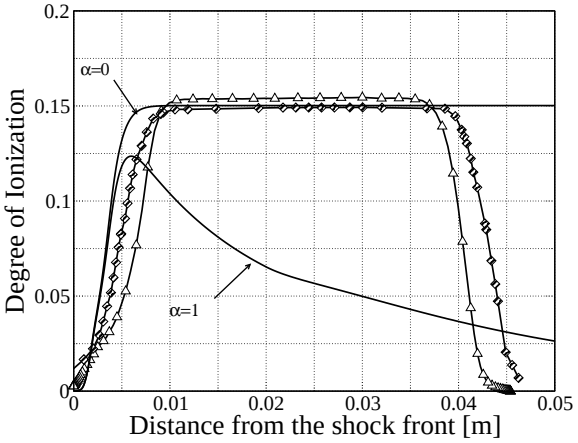

7.2: **Ionization degree profiles: CR model with escape factor values of 0 and 1 (unbroken line), Laura code (34) (line with diamonds), and Johnston's results (37) (line with triangles).**

Figure 7: 1636 s case.

In Fig. 7.1, we show profiles of the translational temperature and the molecular nitrogen vibrational temperature obtained by means of our CR model (T and T_{vN_2}) and of the two-temperature reference models (T and T_v). Noticeable differences are found in the thermal relaxation zone. The post-shock translational temperature obtained by means of the SHOCKING code from the Rankine-Hugoniot relations is much higher than the values obtained by the means of the Laura and DPLR codes and closer to the value obtained by Johnston who used a discrete boundary condition (shock slip condition). Another possible source of discrepancies is the absence of dissipative effects in the CR model. The vibrational temperature obtained by the means of the CFD codes is higher than the frozen value. Fair agreement can be observed among all the results for the vibrational temperature of N_2. This is very important seeing its close association with radiation, electronic excitation, and electron density(Park).
The optical thickness of the medium plays an important role in our simulations. The upper curve (labeled $\alpha = 0$) represents the optically thick case, and the lower curve (labeled $\alpha = 1$), the optically thin case. A lower temperature is obtained for an optically thin medium since the flow energy is depleted by radiation.

In Fig. 7.2, we compare the results obtained for the ionization degree. In the case of an optically thick medium, it reaches a plateau; a fair agreement is found with the literature. Large differences are found when radiative cooling is taken into account since it reduces the degree of ionization. Our model predicts that the ionization process is more rapid than the model implemented into the LAURA code and into the viscous shock layer code.

1.2.8 Electronic energy populations

In Fig. 8, the electronic energy level populations are shown at 0.5 cm from the shock front, for an electron temperature value of 12 883 K. We clearly see that the low electronic energy levels tend to follow a Boltzmann distribution at the electron temperature, whereas, close to

the ionization limit, the excited electronic states approach a Saha distribution at the electron temperature. Since the channels between the low and high lying electronic states exhibit finite ionization rates, a lack of free electrons may result in depleted populations for the highly excited states. The distribution is no longer of Boltzmann type and the electronic temperature is no longer defined.
The departures from the Boltzmann distribution, which are of the same order of magnitude for atomic nitrogen and atomic oxygen, tend to reduce the radiative contribution to the overall heat flux in the earlier parts of the trajectory. For this reason, attempts to estimate the radiative flux assuming a Boltzmann distribution among electronic levels might lead to an overestimation of this heat flux.

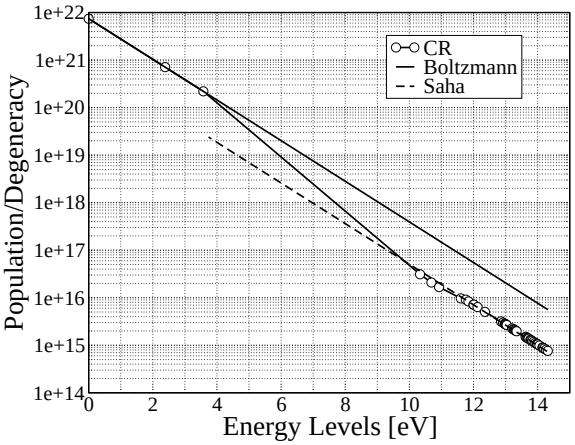

8.1: **Atomic nitrogen.**

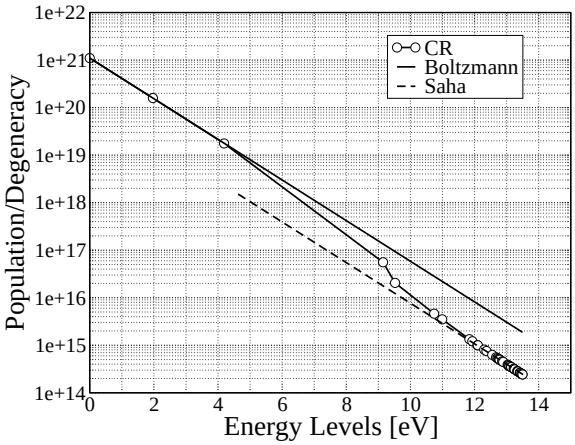

8.2: **Atomic oxygen.**

Figure 8: 1636 s case, 0.5 cm from the shock front. Electronic energy level populations [m^{-3}]: CR model (line with circles), Boltzmann distribution (unbroken line), and Saha distribution (dashed line).

1.2.9 Analysis of the Fire II 1643 s case

In this section, we analyze a trajectory point close to peak heating. Figure 9.1 shows that the thermal nonequilibrium effects are located in a very narrow region near the shock. The electronic energy level populations of atomic nitrogen at 0.5 cm from the shock are given in Fig. 9.2. It is interesting to mention that these populations follow Boltzmann distributions in the entire domain. These results are explained by the values of the post-shock pressure p_2 given in Table 3, much higher than for the first two trajectory points. At high pressures, the plasma is dominated by collisional processes; thermal relaxation is enhanced and the electronic state populations tend towards Boltzmann distributions.

1.3 Conclusions

In this work, we have studied the departure of the atomic electronic energy populations from Boltzmann distributions for onedimensional air flows obtained in a shock-tube. The operating conditions are taken from three points in the trajectory of the FIRE II flight experiment at 1634 s, 1636 s, and 1643 s elapsed time from the launch. The results have been obtained by means of a multi-temperature fluid model fully coupled with an electronic-specific collisional radiative model. We have compared the flowfield quantities and electronic energy populations

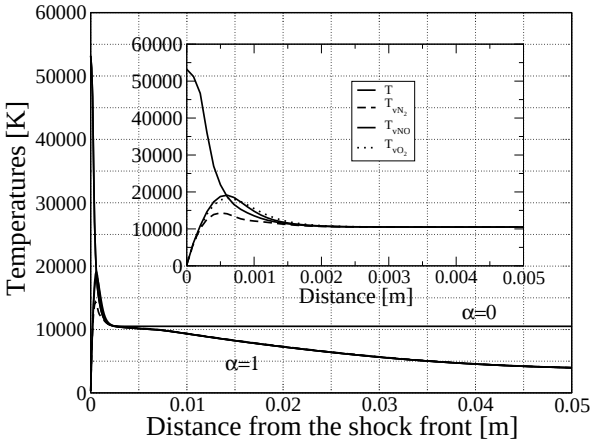

9.1:

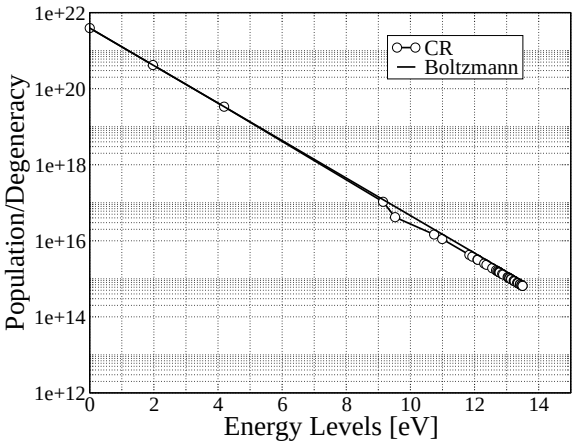

9.2:

Figure 9: 1643 s case. (a) Temperature profiles with escape factor values of 0 and 1. (b) Electronic energy level populations for atomic nitrogen [m^{-3}]: CR model (line with circles) and Boltzmann distribution (unbroken line), 0.5 cm from the shock front.

with literature (34; 37) and found a good agreement. We have also found that, for the first two points of the trajectory (1634 s and 1636 s), the electronic energy level populations of the N and O atoms depart from Boltzmann distributions since the high lying bound electronic states are depleted. The analysis of the last trajectory point (1643 s) reveals instead a Boltzmann distribution among the electronic levels.

An analysis of the state of the flow for the first flight condition (1634 s) led us to the conclusion that the excited species of atoms satisfy the quasi-steady-state assumption, except for the two metastable states. As a consequence, the global rate coefficients and free electron energy loss terms could be derived in the steady state based on our model, considering however the metastable states as separate pseudo-species governed by their own chemical-kinetic mechanism. Moreover, the validity of the standard QSS approach widely used by the aerospace community has been tested; the results obtained by means of our full CR model and the standard QSS model are found in good agreement. It is important to mention that the full CR model is more general, since the parameters governing the free-electron energy losses by electron impact ionization are obtained from the expressions for the reaction rates intrinsic to the model, without any a priori hypothesis.
Finally, we have shown that the populations of high-lying excited states of atoms obtained by using the rates of Park (51) for electron-impact excitation and ionization reactions are up to two orders of magnitude higher than the populations obtained by using the rates of Bultel et al. (11), consistent with the result of Johnston (37).

2 Comparison with EAST experiments

The analysis presented in this section has been carried out in collaboration with Dr. Yacine Babou (Researcher Engineer at von Karman Institute for fluid dynamics).

Introduction

The present work is committed to the partial validation of the *electronically specific* collisional-radiative model, thoroughly described in § 1, ((11; 49; 48)) (indicated in the following as Abba model), against the recent measurements (28), given in Ref. (36) and performed in the EAST shock tube facility. The analysis allows us to extract useful information concerning the accuracy of the collisional and radiative mechanisms used and at the same time to gain some insight on the chemico-physical processes occurring behind strong shock waves.

In section § 2.1, we briefly recall the features of the physico-chemical models implemented in the SHOCKING code and we describe the modifications introduced in the ABBA model in order to improve the modeling of the excitation and ionization by electron-impact and to enhance the agreement with the experimental results. The choice to focus our attention on the atomic processes is justified by the fact that, at high temperatures and for high speed re-entry ($\geq$ 10 $km\ s^{-1}$), the contribution of the radiative component to the heat flux is dominated by atomic lines and continuum radiation (37; 6; 36; 49), the molecules being almost completely dissociated in this temperature range. More extensive description of the model employed can be found in Ref. (49; 48; 11)

The radiation prediction, described in section § 2.2, is carried out on the basis of the advanced tools available at the EM2C laboratories (Le laboratoire d'Energetique Moleculaire et Macroscopique, Combustion, www.em2c.ecp.fr), based on the spectroscopic database dedicated to the study of the radiative transfer inside air plasmas under chemical and thermal equilibrium in the temperature range $300 - 25000\ K$ (17; 18; 23). Atomic lines which constitute the focus of the present investigation have been taken from the NIST database (45).The influence of the velocity and the pressure on the radiative signature of the plasma is analyzed using high resolution spectra and radiative source strength.

The section of results § 2.3 is divided in three parts. We first analyze the physico-chemical state of the plasma in the post-shock relaxation zone in terms of temperature profiles and population densities of the electronic levels of the atoms.
We move then to the analysis of the radiative properties of the shock layer, comparing the simulated radiative signature with the experiments. Considerations on the optical properties of the gas, i. e. optical thickness, are also discussed in this part of the manuscript.
In the last part of the section we focus our attention on the influence of the chemical kinetics on the results. In this part a new set of cross sections for the elementary processes of excitation and ionization is also tested. Moreover the influence of the shock speed on the radiative intensity is investigated, analyzing in detailed the influence of the ionizational nonequilibrium on the radiative signature.

2.1 Physico-Chemical modeling

Numerical predictions are carried out by making use of two different codes: SHOCKING code(48; 49) for the flowfield calculations and the radiation code solver developed at EM2C

for the study of radiative processes.

The first numerical tool is used to model the chemico-physical phenomena taking place in the relaxation zone behind a shock waves, whereas the second code is used to model the radiative signature of the high temperature gas.

SHOCKING describes the post-shock relaxation area by means of 1D Euler equations fully coupled with a set of equations describing the thermal relaxation processes (§1.1.7). In the present contribution only one temperature T_V is used to describe the nonequilibrium relaxation process for vibration and electronic excitation processes of the molecules, and therefore a common temperature is used to describe the internal vibrational and electronic energy stored into the gas.
When equilibrium among the vibrational levels of all the molecules is assumed the vibrational and electronic conservation equation takes this form:

$$\frac{\partial}{\partial x}\left[\rho u\left(e^V + y_e e_e + \sum_{i\in\mathcal{E}} y_i e_i^E\right)\right] = -p_e\frac{\partial u}{\partial x} + \sum_{i\in\mathcal{E}} M_i\dot{\omega}_i e_i^E - \Omega^I - \Omega^E + \Omega^{ET} + \sum_{m\in\mathcal{V}} M_m\,\dot{\omega}_m e_m^V + \Omega^{VT} \tag{17}$$

The collisional radiative model is coupled with the flowfield model to determine the evolution of the electronic population densities of the atoms. The populations of the internal levels of the atoms are modeled by means of a CR model writing a master equation for each electronic level considering it as separate pseudo-species. Conservation equations of mass, momentum, global energy, vibrational and free-electron-electronic energy are solved simultaneously, as opposed to Lagrangian methods (44) and quasi-steady-state approximations (7; 37) where the electronic populations are determined subsequently to the flow calculation.

2.1.1 Kinetic mechanisms

Behind strong shock waves population of the electronically excited states is assumed to depart from equilibrium distribution (Boltzmann) and to be governed by finite rate chemical kinetics. A detailed description of the processes that populate and de-populate the electronically excited states can be found in Ref. (20; 51). In the present work, rate constants for elementary processes for radiative and kinetic transition are taken from Ref. (11). Moreover in order to assess the influence of the kinetic processes on the results we have decided to modify the kinetic data set that governs the excitation and ionization by electron impact. Since the electronic excitation of atoms directly affects radiation, a direct comparison with the measured intensity diagrams can give an idea of the accuracy of the model used. The importance of the atomic line radiation for high speed entry conditions has been discussed in Ref. (6; 36) and justifies the need for a sensitivity study.

2.1.2 Excitation by electron impact

The nonelastic cross sections for ionization and excitation by electron impact exhibit a surprising degree of regularity and have been the subject of considerable theoretical research (46). Several "universal" formulas for these cross sections have been proposed.
The original set of rate constants implemented in the Abba model is based on direct integration of Drawin(25; 24) cross sections. In the following different kinetic mechanisms will be tested:

- Gryzinski cross sections(31) rely on the hydrogenic assumption and are derived based on classical calculations. Although Gryzinski calculations are based on classical mechanics

several ad-hoc assumptions are made in obtaining the final results and so to some extent these results may be view as semi-empirical as Drawin's formula.

- Frost et al.(27) performed R-matrix calculations for atomic nitrogen in the energy region below $50\,eV$. Collision strengths were calculated for optically allowed and forbidden transitions involving energy levels with principal quantum number ≤ 3. Spectroscopic measurements have been performed in the theoretically uncertain near-threshold region.

2.1.3 Ionization by electron impact

Two different formulations (Ref. (24) and Ref. (37)) for the electron impact ionization are used in the present contribution, and both are based on the work of Drawin. The first model is used in the baseline Abba model (11), whereas the second model is used in the CR model of Johnston (37). It is important to notice that a direct comparison of the rate constants shows a difference of 1 order of magnitude for the two models.

2.1.4 Models used in the investigation

The different models for the elementary processes described in the foregoing sections together describe the excitation and ionization processes of the atomic species. In the present section we briefly describe each of the models used in the investigation.

Abba model constitutes the baseline model and has been thoroughly described in Ref. (11; 48; 49)

Abba TCNQ uses the set of kinetic data provided by Abba but the energy exchange source terms among internal energy modes have been changed with respect to the Abba models. In particular, this model accounts for preferential dissociation phenomena (29), diffusion model of Park (51) for the VT relaxation and we make use of the electronic energy reactive source term described in Ref. (37).

Abba Modified is based on the Abba model, however an updated set of reaction rate constants is used for the excitation and ionization of atoms by electron impact. In particular, the model of Frost et al.(27) has been used for the excitation of the ground state and the two metastable states to the upper states. For the missing reaction we resort to the work of Gryzinski (31). Ionization by electron impact is modeled as described in Ref. (37)

Moreover in order to assess the influences of the each set of reaction we define the following model *Abba Frost* and *Abba Gryzinski*. In order to clarify the differences among the different tools of the investigation we summarize in Tab. 4 all the features of the kinetic models.

2.2 Radiative properties prediction

The radiative signature of the considered plasma being considered is determined on the basis of the advanced tool developed and available at the EM2C laboratory and partially presented in various contributions (see (62; 18; 58; 17; 23; 2; 40; 3)). This tool allows for calculation of non equilibrium O-C-Ar-N mixture plasmas at high temperature, high resolution emission and absorption spectra due to bound-bound, bound-free and free-free transitions over a wide spectral range from the VUV to the far Infrared. Without entering into details, this tool includes an exhaustive and reliable spectroscopic data base, described in Refs. (18; 17) for O_2-N_2 mixtures,

combined with suitable emission and absorption expressions, presented in Ref. (40) in the frame of a two temperature description of the thermodynamic state of the plasma. For all the radiative mechanisms, except for N and O bound-bound transitions radiative properties are calculated using expressions provided by Ref.(40). According to the state-by-state description considered here for N and O energy level distributions, adaptations were carried out in some extent for the calculation of radiative properties due to the bound-bound transitions. Similar improvements may also be made for the photo-ionization since detailed absorption cross-sections are available in the TOPBASE databases (67), but are not required in the present contribution since the present work is dedicated to the N and O radiative bound-bound transitions.

For N and O radiative bound-bound transition from an upper level i to a lower level j the corresponding emission and absorption coefficients are obtained using the usual expressions :

$$\eta_\sigma = n_i \frac{A_{ij}}{4\pi} hc\sigma_{ij} f(\sigma - \sigma_{ij}) \tag{18}$$

$$\kappa_\sigma = (n_j B_{ji} - n_i B_{ij}) h\sigma_{ij} f(\sigma - \sigma_{ij}) \tag{19}$$

where n_i (respectively n_j) is the population of the upper (respectively lower) level; A_{ij}, B_{ij} and B_{ji} are the Einstein coefficients respectively for spontaneous emission, induced emission and absorption processes; σ_{ij} is the transition wave number and $f(\sigma - \sigma_{ij})$ is the spectral line profile shape which accounts for collisional and Doppler broadening; h and c are the Planck constant and the light velocity. Wave number and Einstein coefficient values are taken from the NIST (45) databases. The collisional line width, including van der Waals, resonance and Stark broadening was estimated in the frame of the semi-classical adiabatic approximation (see (58)).

Note that the code SHOCKING provides density numbers for "pseudo" electronic levels corresponding in reality to grouped electronic levels according to their fine structure energy levels and to their electronic configurations for highly excited levels. For electronic levels i belonging to the grouped level k, the required population n_i for individual levels is calculated assuming that the levels i are in Boltzmann equilibrium at T_V according to :

$$n_i = n_k \frac{g_k}{g_i} exp\left(-\frac{E_k - E_i}{k_B T_V}\right), \tag{20}$$

where the population n_k is provided by the CR calculations. The energy E_k of the group (respectively the degeneracy g_k) is related to the corresponding individual energy levels E_i (respectively degeneracy's g_i) through $E_k = \frac{\sum_i g_i E_i}{g_k}$ (respectively $g_k = \sum_i g_i$).

For the other levels which are not considered in the Abba model (energy levels above 14.31962 eV for N and above 13.48156 eV for O), we assumed that they are in Saha-Boltzmann equilibrium with the free electrons, thus the population n_i of the energy level E_i is determined according to :

$$n_i = N_A N_{el} \left(\frac{h^2}{2\pi m k_B T_V}\right)^{\frac{3}{2}} g_i \frac{exp\left(-\frac{(E_i - E_{ion})}{k_B T_V}\right)}{2Q_A(T_V)} \tag{21}$$

where N_{el} and N_X designate the concentration of respectively the electrons and the atomic specie A (which is O or N). $Q_A(T_V)$ is the partition function of the atomic specie A; g_i is the degeneracy of level i; E_{ion} is the ionization energy corrected from the Debye ionization lowering and m is the reduced mass.

2.3 Results

The investigation of the reliability of the physico-chemical models considered in this study is carried out by comparing the predicted post-shock radiation to the measured post shock

radiation for relevant test conditions. The suitable measurements for this purpose are provided by the recent experiments carried out with the NASA Ames EAST facility. The EAST facility is a 10.16 diameter shock tube with an electric arc-heated driver. The arc in the driver is supported by a capacitor bank which can store up to 1.24 MJ of energy heated at 40kV (see Refs. (63; 64)).

The EAST experiments considered in the present work were dedicated to the absolute measurements of the intensity profile behind an air moving shock. The pressure of the driver gas (He/Ar mixtures) was maintained at 0.1 and 0.3 Torr, and the velocity was targeted to 10 km.s^{-1} and measured with an uncertainty of 1.5%. The intensity emitted in the normal direction to the propagation as the shock passed by the test section window was recorded using optical benches including two 0.3 m imaging spectrographs coupled at the exit focal plane, along with various intensified cameras for measurements in UV, visible and infrared spectral ranges. The spectral resolutions of the cameras ranged from 0.08 to 2 nm and with exposure time ranging from 0.015 to 0.98 μs. Detailed description of the measurement campaign, including the test matrix and the instrumentation, is documented in Ref.(28), and the calibration procedures and sample error analyses are reported in Ref.(8; 30).

The EAST measurement campaign was very fruitful, and the recorded spatially and spectrally resolved spectra are still under post-processing; therefore only few data are published. Since they are still classified, experimental data considered in this study are taken from the literature in a crude manner. We used the intensity profiles measured in the spectral range 700-1020 nm and available and analyzed in Ref.(36) for the test cases documented in Table 5. The experimental data analysis has revealed that the radiation is mainly due to N and O bound-bound transitions. The measurements are presented in terms of spatial absolute intensity profiles $I^{exp}_{\Delta\lambda}(x)$ spectrally integrated over a suitable wavelength range $\Delta\lambda$ to emphasize the contribution to the emission of well defined electronic levels. The spectral ranges and the corresponding upper grouped levels are detailed in Fig. 10. For the high pressure cases (0.3 Torr), the radiation was found to rapidly achieve the equilibrium. For the low pressure cases (0.1 Torr), the distribution of the observed N and O emitting energy levels was found to be different from the Boltzmann one along the distance away from the shock up to 4 cm. The measured radiation contains useful information as far as the population of some excited N and O atomic levels is concerned, which allows for the aimed investigation of the reliability of the considered kinetic models (see Sec. 2.1) for the prediction of the non-equilibrium post-shock excitation as well as relaxation stages. The temperature and population profiles predicted on the basis of the models described in Sec. 2.1, and the resulting radiative properties, determined by combining the tool presented in section Sec. 2.2 to the calculated temperatures and number densities, are presented below. Then, comparisons of the predictions to the measurements are presented and discussed to suggest some possible improvements for the Abba set of data for kinetic reactions involving N and O atoms.

2.3.1 Thermo-chemical state and radiative signature predictions

The aim of the present section is to describe the physico-chemical state of the plasma flow in the post shock region for the test conditions corresponding to Case 3 and 4. In the first part of the section, temperature profiles and composition are presented and discussed whereas the remaining part is devoted to the study of the evolution of the population of excited states and the influence of the excitation model on the results.

Figure (11.1) shows the evolution of the temperature profiles in the post shock region. Across the shock the internal energy modes are assumed to be frozen as well as the chemistry, whereas we use Rankine-Hugoniot's jump relations to estimate post shock pressure, velocity and trans-

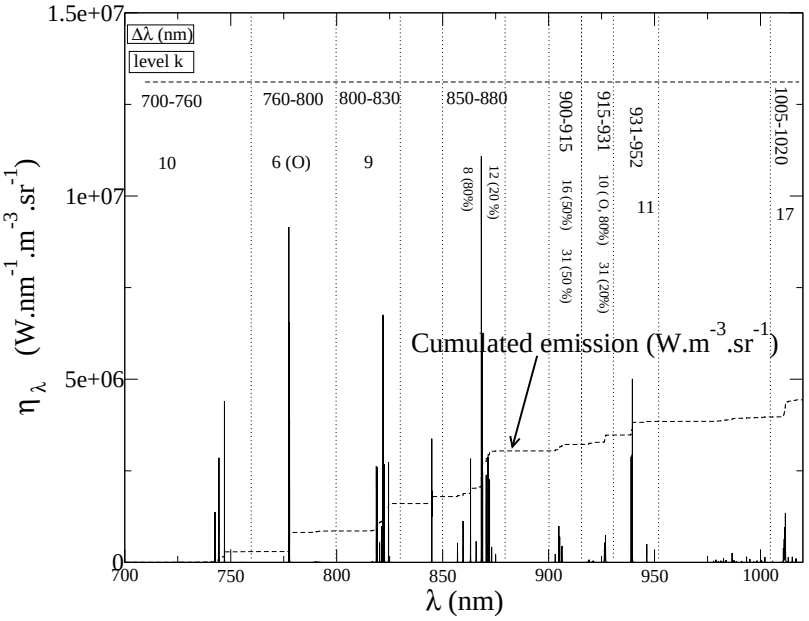

Figure 10: High resolution emission coefficient predicted for Case 1 at 4 cm downstream from the shock. The considered spectral ranges $\Delta\lambda$ are detailed. The corresponding main contributing electronic levels are indicated using the nomenclature of Ref. (48; 49).

lational temperature.
We remind the reader that T_V describes the vibrational and electronic temperature of the molecules and the energy stored in the translational mode of the free electrons. The internal energy stored in the energy modes of the atoms is computed by means of the CR models, which gives directly the populations of the excited states.

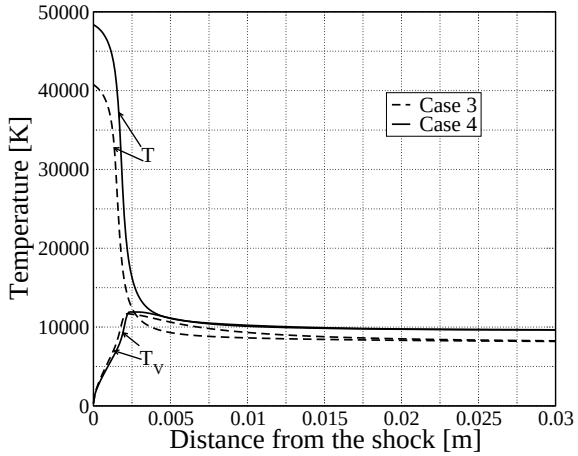

11.1: **Case 3-4. Temperature profiles . Dashed line profiles correspond to flight conditions of case 3. Unbroken lines refer to case 4.**

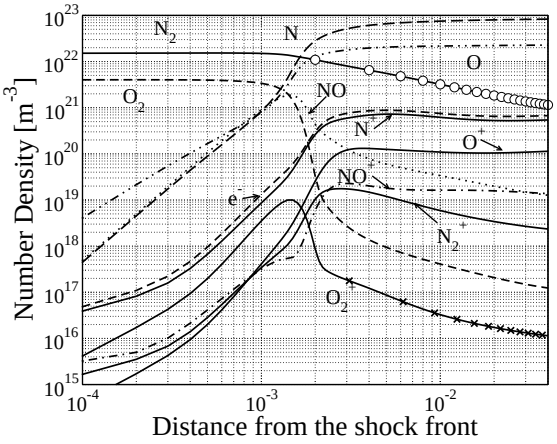

11.2: **Case 3. Evolution of the composition in the post shock area.**

Figure 11: Case 3-4. Post shock temperature [K] and concentration profiles $[m^{-3}]$.

In Fig. 11.2, we examine the evolution of the different species concentrations. Right after the shock molecular oxygen quickly dissociates whereas the dissociation of the nitrogen is slower. At higher shock velocities, however dissociation tends to proceed faster than ionization so that the rate equations for ionization may be decoupled from the dissociation reactions assuming that dissociation is complete.
Since the concentration of N^+ and free electrons are very close in the diagram we can assume that most of the electrons are created by ionization of the atomic nitrogen.

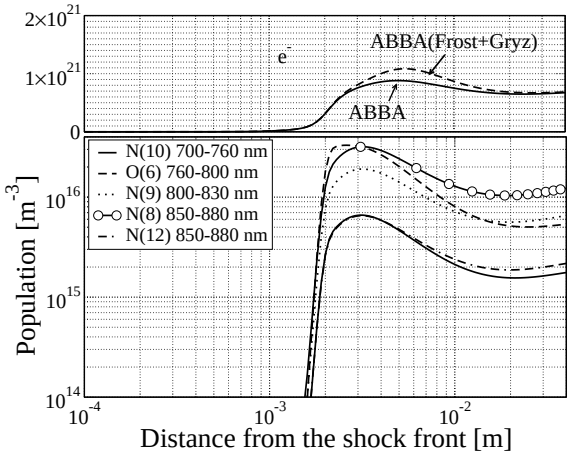

12.1: **Case 3. Populations of electronically excited states.** N(10) (unbroken line), O(6) (dashed line), N(9) (dotted line), N(8) (circle) and N(12) (dash-dotted line)

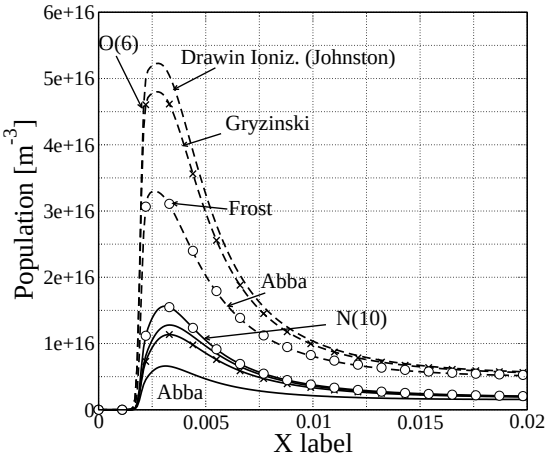

12.2: **Influence of the model on the population densities of** O(6) and N(10) electronic states.

Figure 12: Case 3. Populations evolution of the electronic states of atomic nitrogen and oxygen.

Figure (12.1) shows the evolution of the electronic states of atomic nitrogen and oxygen. As we shall see in the next sections those states are responsible for the bound to bound radiation emitted in the spectral range from 700 nm to 880 nm (Case 1-3). The foregoing spectral range is believed to be almost completely thin(36) for the flight conditions corresponding to Case 3 and this gives us the possibility to have direct access to the population density of the emitting states (with emission measurements) and to validate in this sense the accuracy of the CR model proposed.

Excitation by electron impact is the main channel of excitation of atoms, and electron density has therefore a crucial importance in the evolution of the electronically excited states. Electron impact excitation reactions are fast and the populations of excited electronic states rapidly increase. The upper states are then depleted, in particular by ionization and spontaneous emission, which explains the maximum found in the population profiles. The maximum in the population corresponds to a maximum in the radiation that, as we shall see, exhibits the same peak in the nonequilibrium zone after the shock.

The population profiles for the atomic oxen (O(6)) and (N(10)) is depicted in figure (12.2). The use of the Frost's rate constants does not affect the population profile of O(6) as expected since the set of reaction rates proposed by Frost concern the excitation from ground and metastable states to the excited states of nitrogen atoms.
The Gryzinski cross sections instead promote the excitation of O(6) enhancing the overshoot in the population density profile. Electron impact ionization reactions do not seem to affect in

significant way the evolution of the profile in the overshoot region.

2.3.2 Comparisons with experiments and analysis

For comparisons with the measured intensity profiles $I^{exp}_{\Delta\lambda}(x)$ taken from (36), the intensity profile was first predicted using the radiative transfer equation for the intensity resulting from a constant property line of sight. Assuming that the radiation coming from the wall at the opposite side of the window is negligible in $\Delta\lambda$, the intensity profile $I_\lambda(x)$ for a given location x may be written as :

$$I_\lambda(x) = \frac{\eta_\lambda(x)}{\kappa_\lambda(x)}(1 - e^{-\kappa_\lambda(x)D}) \tag{22}$$

where the shock diameter D is assumed to be equal to the shock-tube test section diameter 10.16 cm; $\eta_\lambda(x)$ and $\kappa_\lambda(x)$ are the emission and absorption coefficients at the location x. The intensity $I_\lambda(x)$ was then spectrally integrated over well defined narrow wave length ranges $\Delta\lambda$ detailed in Fig. 10, and the intensity profile $I^{sim}_{\Delta\lambda}(x)$, simulated under experimental conditions, was obtained by convoluting the resulting spatial profiles of the integrated intensity to a gate function normalized to one to take into account the non negligible spatial smearing due to the post-shock transit during the acquisition time :

$$I^{sim}_{\Delta\lambda}(x) = \frac{1}{\Delta x}\int_x^{x+\Delta x}\left(\int_{\Delta\lambda} I_\lambda(x')\, d\lambda\right)\, dx', \tag{23}$$

where Δx is equal to the shock velocity v_s multiplied by acquisition time τ_{acq}.

The overall comparisons, for the four cases investigated, are gathered in Figs. (13) and (14) to outline some peculiarities of the predictions. The high pressure cases 1 and 2 are characterized by a fast and abrupt rise of the intensity profile corresponding to the excitation stage of the post shock flow. Also, we observe that at higher velocity, the equilibrium stage (or plateau) is reached earlier. For the low pressure case 3 (see Fig. (13) (on the right)), the intensity presents a pronounced peaked shape profile located at about 0.7 cm, followed by a slightly decreasing profile indicating that the flow still may be in the relaxation stage at 4 cm. For the low pressure case 4, the intensity profile, shown in Fig. (13) (on the right) increases slowly over the whole spatial range suggesting that, similarly to Case 3, the equilibrium may not yet be achieved at 4 cm possibly due to a lower number of collisions than in the higher pressure cases. The intensity profile presents also a little burst, which is not predicted, situated at about the same location as the peak observed for Case 3.
The measured intensity profiles for Cases 2 and 4 are compared to the predicted profiles using the Abba baseline model with the assumption that the plasma is optically thin ($\Lambda = 1$) and, alternatively that the radiated energy is fully absorbed in the VUV ($\Lambda = X$) and in the overall spectral range ($\Lambda = 0$). For $\Lambda = 1$, the population of electronic levels is ruled by collisional processes and by the only possible radiative de-excitation processes from higher levels since the radiated energy is not absorbed and completely escapes the plasma. This leads to the decrease in the population of the emitting, (*radiative cooling*) beyond a distance at about 1 and 2 cm, for Cases 2 and 4 respectively. This is in contrast to the calculations for $\Lambda \neq 0$ for which the contribution of the radiation balances the collisional depletion. The prominence of the radiative process within the VUV spectral range in the balance is revealed by the agreement between the $\Lambda = 0$ and $\Lambda = X$ calculations. The considerably flat shape of the measured profiles far behind the shock is attributed to the negligible radiative energy escaping. Comparisons with optically thin calculations show that the excitation as well as the plateau regions are significantly thick for Case 2 (similar features were observed for Case 1). Cases 3 and 4 were found to be only

slightly thick and can be reasonably considered as thin, except for the spectral range 760-800 nm corresponding to the well known oxygen triplet transitions (as it will be shown below), and in a less extent for the spectral range 931-952 nm.

The influence of the kinetic models considered for the ionization and dissociation mechanism is shown in Figs. 14 for the cases 1 (on the left) and 3 (on the right), where the calculations obtained for $\Lambda = 0$ are compared to the measurements. For the high pressure case 1, a slight influence is observed in the rise of the radiation, corresponding to the non equilibrium stage of the flow confirmed by the departure to the Boltzmann Abba Modified calculations. The influence for the high pressure case 2 was also found to be weak. The influence of the kinetic models is more pronounced in the peak for the low pressure case 3 whereas it remains weak in the quasi-plateau region and the Abba Modified calculations are found to be higher than the Abba profiles. Also, the peak region is characterized by a strong departure of the measurements and calculation to the Boltzmann Abba Modified calculations. The calculations disagree almost by 50% in the peak region and agree in the plateau. Despite a disagreement with the measurements over the whole spatial range, the comparison with the experiments suggest that the Abba Modified, based on updated kinetic models for ionization and excitation processes, can be considered as an improvement. The influence of the model Abba TCNQ used for the thermal relaxation (see Sec. 2.1) is also presented in Fig. 14 and was found to be too weak for the overall cases to justify a refined investigation, in comparisons to the effect of the kinetic models. The overall comparisons show a quite satisfactory agreement except for Case 3, however discrepancies with the measurements remain acceptable (less than 50 % for the Abba modified calculations). For Case 2, the measurements remain over the entire spatial range between the intensity profiles obtained for velocities $v_s - 1.5\%$ and $v_s + 1.5\%$ (corresponding to the experimental uncertainties on the velocity). The measured profile for Case 1 belongs to the $v_s \pm 1.5\%$ profiles range only in the plateau region whereas some discrepancies are observed in the excitation stage. The calculated intensity profiles for Case 4 are slightly underpredicted. Nevertheless, the profile calculated with $v_s + 1.5\%$ is in quite good agreement with the measurements although the intensity burst at about 0.7 cm is not reproduced.

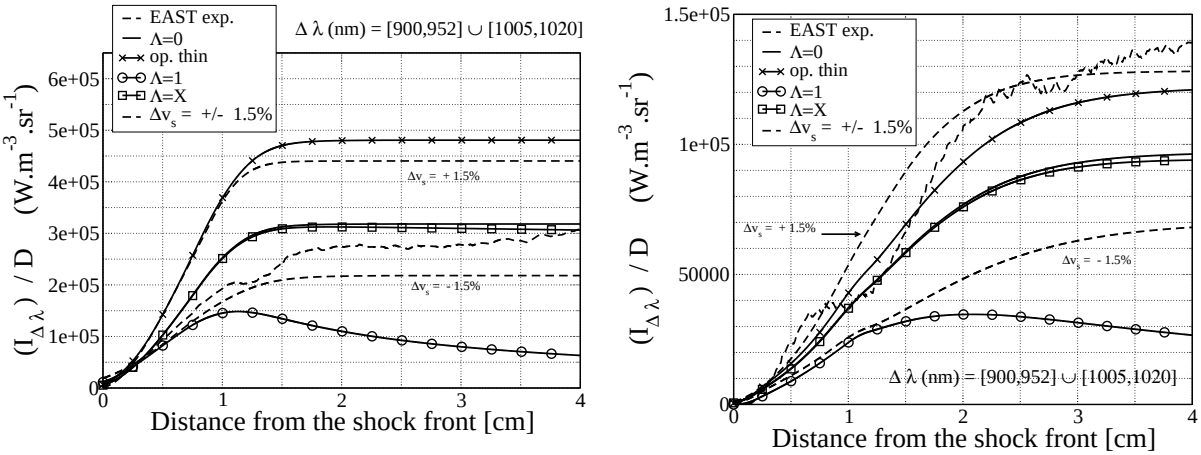

13.1: **Case 2. Shock speed 9880** $m.s^{-1}$

13.2: **Case 4. Shock speed 10340** $m.s^{-1}$

Figure 13: Case 2-4. Comparison among experimental and simulated radiative intensity profiles.

The possible reasons for the observed disagreement may have various sources. The influence of the uncertainty of $\pm 1.5\%$ on the velocity measurements has a significant effect as it

was shown. The uncertainties on the Einstein coefficients (which remain lower than 10 % for the most important transitions) and on the Stark broadening width (which acts mainly on the pronounced optically thick cases 1 and 2) are not sufficient to explain the disagreement obtained for the low pressure cases. The kinetic models have also revealed a important influence on the predictions for the non equilibrium regions.

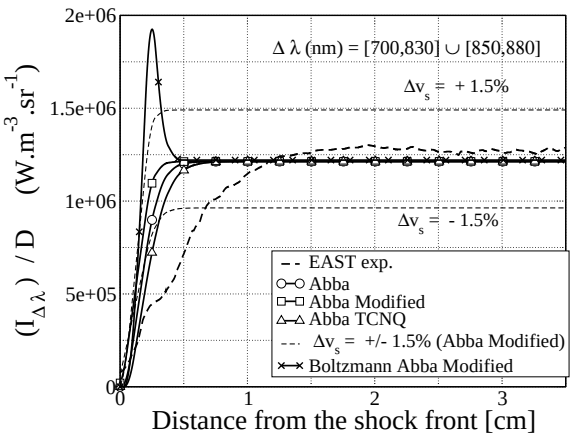

14.1: **Case 1. Shock speed 9165** $m.s^{-1}$

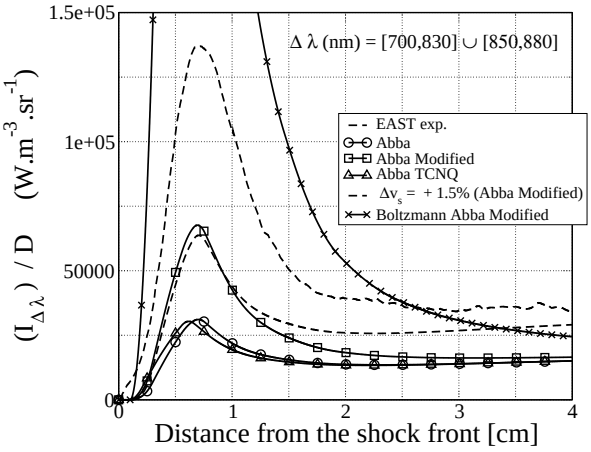

14.2: **Case 3. Shock speed 9989** $m.s^{-1}$

Figure 14: Case 1-3. Comparison among experimental and simulated radiative intensity profiles.

The impact of the different kinetics models considered (see Sec. 2.1), on the population density of the excited levels is detailed in Figs. (15-16) for Cases 3 and 4. The intensity profiles predicted in two narrow spectral ranges corresponding to the N(10) and O(6) levels for Case 3 and N(31), O(10) for Case 4 and are also compared to the experiments. The calculations were performed by combining the Abba baseline model with the various updated kinetic models for the ionization and excitation combinations presented in Table 5.

The analysis of Case 4, in Figure (15), shows rather good agreement with the experimental data. The distance needed to reach the plateau is the same for experiments and numerical simulation. The same figure presents results obtained neglecting the self-absorption, leading to the conclusion that the optical thickness of the gas in this spectral range is negligible. The influence of the model for this case are found negligible since all the volumetric emission profiles are overlapped for the different kinetic mechanisms.
As far as this case is concerned our results seem to match quite well with the prediction given in reference (36), since the departures among the simulated curves and the measured ones are similar.

Figure (16.1)-(16.2) describe the evolution of the radiative signature produced by N(10) and O(6) respectively. We notice a different behavior for the two atomic lines, while the nitrogen atomic line is not strongly self-adsorbed, the O triplet line depicted in Figure (16.2) is strongly self-adsorbed. Focusing our attention on Figure (16.1) we can see that the baseline Abba model underestimates the peak of radiative intensity by 83%, whereas the modified Abba underestimate the peak region by 66%. The improvement is mainly due to the use of rate constants computed by Frost et al.(27), this can be argued by the fact that adding the Gryzinski's cross sections have a negligible impact on the results. Figure (16.2) shows perfect agreement with the experimental data for the thin case and the modified Abba model. However when the self-

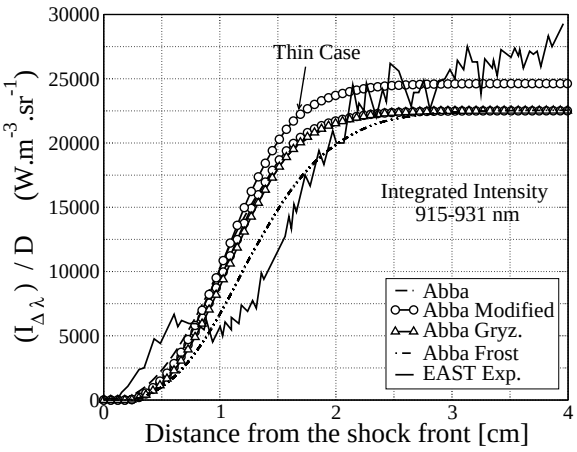

Figure 15: Case 4. Comparison among experimental and simulated radiative intensity profiles.

absorption is accounted for the same kind of under-prediction obtained for the other nitrogen line can be observed. As expected Frost's model plays no influence on the results, as expected since it applies only for the atomic nitrogen. In this case however the modified Abba model can take advantage of the cross sections due to Gryzinski that accounts for the increase of the peak in the radiation intensity.

Globally we can conclude that the modified Abba model improves the agreement with the experimental results performed on the EAST facility.

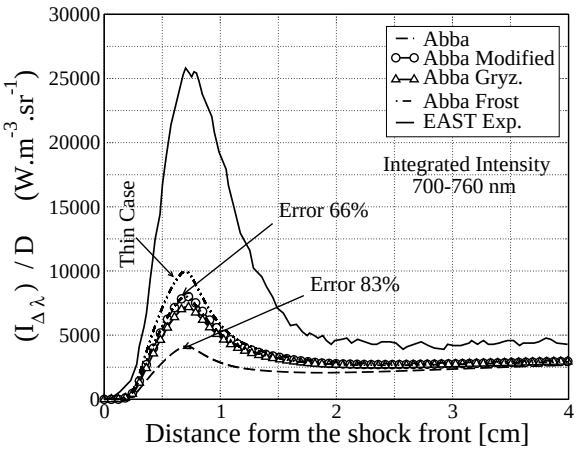

16.1: **Spectral integrated profiles** $\Delta\lambda = 700 - 760$.

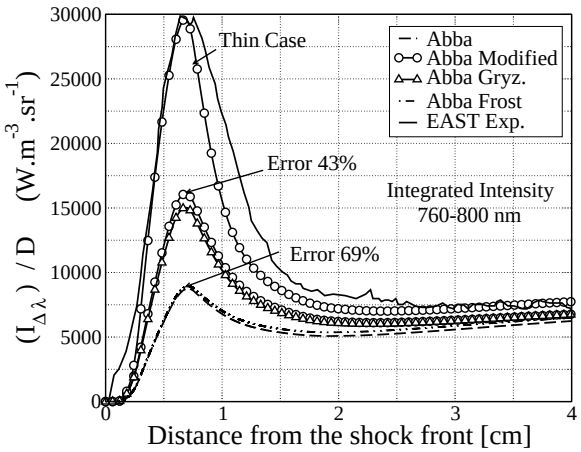

16.2: **Spectral integrated profiles** $\Delta\lambda = 760 - 800$

Figure 16: Case 3. Comparison among experimental and simulated radiative intensity profiles.

Further insight into this comparison is gained from inferring the number densities of the radiating levels from the measured intensities as explained in Ref. (36). The results are plotted in Figure (17.1-17.2), where the normalized population, i.e. the population of the electronic levels divided by the degeneracy of the corresponding level, is depicted as a function of the energy expressed in eV. Figure (17.1) describes the population densities of the electronic states of atomic

nitrogen at a distance of 0.65 *cm* from the shock front and corresponds to the shock condition of Case 3. Figure (17.2) describes the excitation of the atomic nitrogen for the shock conditions of Case 4 and at a location of 1 *cm* from the shock front. The consistent under-prediction of the measurements is indicated by the underpopulation of the corresponding radiating levels and is in good agreement with the numerical predictions. Generally speaking the predicted population densities are underestimated by (50%) for Case 3, whereas the agreement is quite good for Case 4.

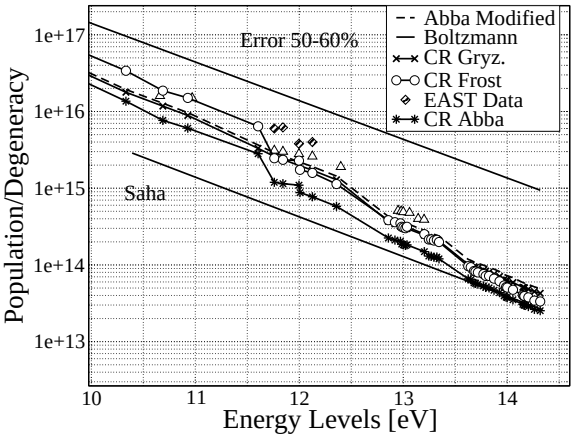

17.1: **Case 3. Normalized population of the electronic states of atomic nitrogen at 0.65 cm from the shock front.**

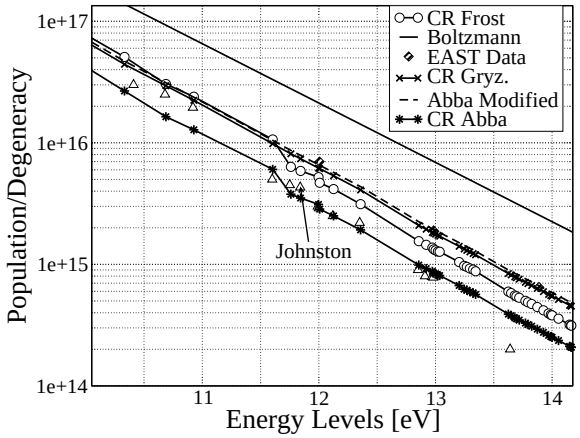

17.2: **Case 4. Normalized population of the electronic states of atomic nitrogen at 1.0 cm from the shock front.**

Figure 17: Electronic energy level populations [m^{-3}]: CR model Abba Frost (line with circles), Boltzmann distribution (unbroken line), and Saha distribution (dashed line).

As a concluding discussion, the strong influence of the velocity on the feature of the radiation for the low pressure case is investigated below. For high speed flight conditions molecules quickly dissociate and radiation is mostly produced by atoms. Atomic radiation depends on the electron density as well as the free-electron temperature (in our case T_V), which are affected by the nonequilibrium ionization process (52). In order to correctly describe the radiation mechanism an accurate description of the ionization process is required.

It is well known (52) that the number of chemical reactions involved in the nonequilibrium ionization processes occurring in air shock increases with the velocity. At low velocity, the electrons are mainly produced by the associative ionization process, i.e. $N + O \rightarrow NO^+ + e^-$, since the direct ionization of N and O is forbidden for energy reasons. The efficiency of this process is determined by the decrease in the ionization threshold resulting from the chemical bond energy of the molecular ion (20).

At intermediate velocity (about 8-9 $km.s^{-1}$), charge exchange is added to the first process. Let us consider for example the following reaction, $NO^+ + N \rightarrow NO + N^+$. When the rates for charge exchange are high, a great amount of N^+ is formed, at expenses of NO^+, formed by associative ionization. NO^+ reacts with N, produced by dissociation of N_2. In these conditions, the production of N^+ leads to a decrease of the role of the direct formation of N^+ by electron impact on N, and as a result an increase of the ionization distance can be observed.
For high velocity, the density of the produced electrons becomes sufficient to activate the electronic avalanche through the electron impact ionization $N + e^- \rightarrow N^+ + 2e^-$, leading to the

exponential rise of the electron density. It is interesting to note that the impact that this mechanism has on the ionization rate is limited by the loss of the electronic thermal energy during the electron impact ionization process (51; 20; 52). Indeed a high rate of ionization suppresses the electron thermal energy by this mechanism. The evolutions of the calculated intensity profiles and electron density, in the velocity range 9-10 km.s^{-1}, are given in Fig. (18.1)-(18.2) respectively, with the Abba-Modified model. The two sets of profiles present similar features: at 9 km.s^{-1} they are characterized by pronounced peaked shape in the nearest region after the shock followed by a plateau. Increasing the velocity, it is observed that, the plateau rises much more rapidly than the peak removing the overshoot at about 10 km.s^{-1}.
Similarities in the evolution of electron density (in Fig. (18.2) and population of the excited levels (in Fig. (12.1) is justified by the fact that excitation is mainly ruled by the electron-impact processes because of the high degree of ionization (excited states are in equilibrium with the free electrons).

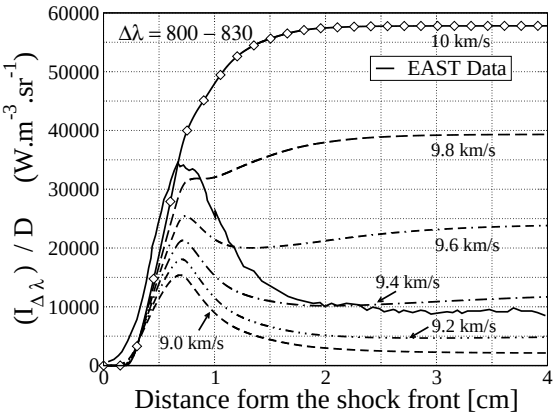

18.1: **Radiative intensity as a function of the shock speed (Ranging from $9 - 10\ km.s^{-1}$).**

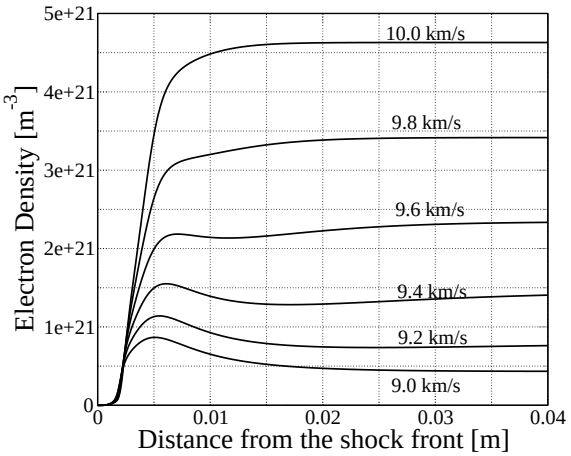

18.2: **Electron density profiles as a function of the shock speed (Ranging from $9 - 10\ km.s^{-1}$).**

Figure 18: Influence of the speed on the radiative intensity profiles.

This transition from a peaked to a monotonic electron density profile is due to the competition between various processes contributing excitation de-activation of the excited states mainly occurring because of the interaction with electrons. The contribution to the net rate of electron production are detailed in Fig. (18.1) and Fig (18.2) for 9 km.s^{-1} and 10 km.s^{-1} respectively. At 9 km.s^{-1}, the net rate becomes negative leading consequently to the observed drop of the electron density at about 1 cm, whereas at 10 km.s^{-1} $\dot{\omega}_e$ remains positive. For the two cases, the negative value for the associative ionization net rate is due to the predominance of the backward reaction induced by a sufficient chemical depletion of the atomic neutral species N and O to reverse the balance.

Increasing the velocity, we observe that this behavior is reduced, and from 9 km.s^{-1} and 10 km.s^{-1} the contribution due to the electron-impact ionization increases 5 times whereas the associative ionization contribution is increased by only 2 times. As a consequence at a certain velocity threshold, where the electron loss by the reverse associative ionization is always compensated the total net rate remains positive after the shock.

Figures (19.1-19.2) show the influence of the kinetic model on the electron impact ionization process. As shown in the figures the major influence is played by Frost kinetic rates which affects

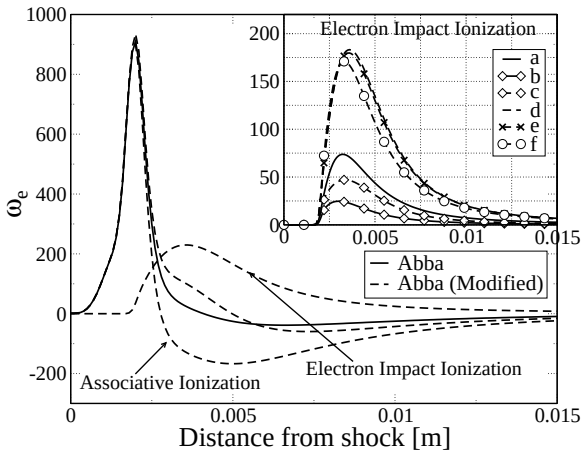

19.1: **Electron production terms** 9 $km.s^{-1}$**. Unbroken lines refer to the Abba model, whereas dashed lines refer to Modified Abba Model.**

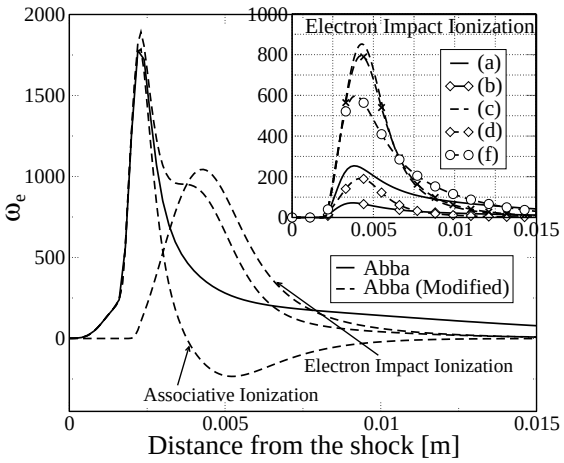

19.2: **Electron production terms** 10 $km.s^{-1}$**. Unbroken lines refer to the Abba model, whereas dashed lines refer to Modified Abba Model.**

Figure 19: Influence of the shock speed on the electron production term $[mole\,.s^{-1}.m^{-3}]$. Where (a) indicates the contribution given by N for Abba.(b) indicates the contribution of O for Abba. (c) Refers to N for Abba Modified. (d) Refers to O for Abba Modified. (e) Refers to N for Abba Gryzinski (f) Refers to N for Abba Frost.

the production of the electrons due to electron impact ionization (by a factor 4). As a result the electron density is also affected (see Fig. 12.1) as well as the radiation intensity profiles.

2.4 Conclusions

In this work, we have studied the relaxation of the atomic electronic energy population distributions for one dimensional air flows obtained in a shock-tube. The operating conditions correspond to four test cases taken from the test campaign carried out at NASA Ames. The results have been obtained by means of a multi-temperature fluid model fully coupled with an electronic-specific collisional radiative model. We have compared the radiative intensity profiles with the experimental data of Ref. (36). We found good agreement for the low pressure run indicated as Case 4 in the manuscript where the flow is in strong nonequilibrium and for the high pressure runs (Case 2 and 3) where the post-shock population density of the excited states follows a Boltzmann distribution.

Differences were found in the results of the comparison for Case 3 where the radiation overshoot is underpredicted by the baseline model tested (Abba). An alternative set of reaction constants have been proposed for the excitation and ionization of atomic species by electron impact. In particular, the use of the kinetic data compiled by Frost et al. (27) seems to reduce the discrepancies with the experimental data.

Part II
Molecules

In the foregoing chapters we have described a simplified ABBA model which allows us to account for nonequilibrium effects in the population of the electronic levels of atomic nitrogen and oxygen. The present section addresses the modeling of the post shock relaxation of atomic and molecular species by means of an electronically specific collisional radiative model.

The last part of the note is devoted to a direct comparison against SPRADIAN07, in terms of population of the excited states of molecules and atoms. We would like to thank C. Park, Hyun S. and Abe T. for providing a copy of the code SPRADIAN07 (vers. 9) used in in this investigation.

3 Collisional Radiative model: molecules

The present section investigates the calculation of the non-Boltzmann electronic state populations for the significant radiating diatomic species present in air shock-layers at lunar return conditions. In particular we analyze N_2 and N_2^+ which are found to be the strongest radiators among the molecular species.

Although it was shown in Ref.(37) that the NO and O_2 molecules contribute to the radiation at lunar-return conditions, it was found that they could be assumed to be populated in a Boltzmann distribution. This assumption is allowable because these molecules do not reach a peak in the nonequilibrium region of the shock layer (unlike the N_2^+ molecule), so their nonequilibrium contribution is small.
Our results seems to confirm the tendency of the molecular oxygen to equilibrate rather quickly after the shock as opposed to the nitric oxide which is underpopulated over all the shock layer.

3.1 ABBA model: molecules

3.1.1 Air mixture

In this study, air is considered as a mixture of N_2, O_2, and their products only: Ar is neglected as well as negative ions. Electronic levels of the atoms are assumed in nonequilibrium as in the previous sections. Moreover in order to investigate the departures of the population of electronic states of molecules from the equilibrium distribution, each of these levels is considered as an additional species whose composition is governed by finite rate chemistry. Here after we write a complete list of species and pseudo-species of the mixture.

- Neutral species: $N_2(1-4)$, $O_2(1-5)$, $NO(1-5)$, $N(1-46)$, and $O(1-40)$,
- Charged species: $N_2^+(1-4)$, $O_2^+(1-4)$, $NO^+(1-5)$, N^+, O^+, and e^-.

Forty-six levels for N and 40 levels for O are taken into account and a total number of 27 levels for the diatomic species. Coupling of these levels through the different elementary processes considered here (see § 1.1.3) allows for the explicit determination of the plasma excitation and its radiative signature without any equilibrium assumption. A list of the electronic levels for molecules and molecular ions is given in Table (6). The overall number of species reads 116.

3.1.2 Elementary processes: Molecules

We now describe the elementary processes included in the model. We limit ourself to a brief description of the elementary processes for the molecules, the models for the atoms being unchanged with respect to the first part of the manuscript (§1.1.3).

The rate coefficients for excitation, ionization and dissociation of molecular species by electron impact have been calculated recently by Teulet(68) and have been used in the present work. The cross section for excitation of molecules under molecular or atomic impact behaves approximately as Lotz(43) therefore this form has been adopted, except in the case when experimental data exist. We have then chosen the rate coefficients compiled by Teulet(69), Capitelli(15) and Kossyi(39). Due to the pressure levels involved in our CR model (which can be employed at high pressure), we have also taken into account the previous processes occurring when a third particle interacts.

Zel'dovitch reactions are known to significantly influence the distribution of nitrogen and oxygen between atomic and molecular systems. Recently, Bose and Candler have updated their rate coefficient using a quasi classical trajectory method performed starting from an ab initio potential surfaces calculation. The proposed rate coefficients have been chosen for this work. Zel'dovitch reactions can contribute to the destruction of O_2 and N_2 and formation of NO.

The direct dissociation and the reverse process by heavy particles impact have to be taken into account. The rate coefficients used are given by Park et al. (56). The rates of dissociation reactions by molecular impact are computed at the average temperature $(T \times T_{vi})^{1/2}$, where index i stands for the molecule being dissociated.

The dissociative recombination DR of the molecular ions is well known to play a very important role in the case of recombining plasmas(Guberman; 12). In addition, the inverse process, the associative ionization, allows in many cases the formation of the first electrons in shock tubes, as well as for the reentry problems, and consequently explains the ionizing situations. In our case since N_2^+, O_2^+, NO^+ are present in the plasma described here, dissociative recombination has to be considered. For more detail we refer to Ref.(11).

3.1.3 Radiative processes

The radiative signature of heated N_2 and O_2 mixtures is mainly due to the spontaneous emission of the N and O atoms. Since our atomic model is based on grouping elementary levels having similar characteristics, the equivalent spontaneous emission probability of each level has to be determined. Related data are taken from the NIST database and given in Table 2) . In total we take into account 45 spontaneous emission lines N and 24 for O.

As far as the molecules are concerned, some states of species mentioned in Table 6, radiate strongly. The β ($B^2\Pi \rightarrow X^2\Pi$) and γ ($A^2\Sigma^+ \rightarrow X^2\Pi$) systems of NO as well as the first positive ($B^3\Pi_g \rightarrow A^3\Sigma_u^+$)) and the second positive ($C^3\Pi_u \rightarrow B^3\Pi_g$)) systems of N_2 and the first negative system ($B^3\Sigma_u^+ \rightarrow X^2\Sigma_g^+$)) of N_2^+ have been considered. Since vibrational equilibrium is assumed for these species the equivalent transition probability for the latter systems is calculated fitting the data calculated by Laux and Kruger(21).

The possible re-absorption of radiation is estimated making use of escape factors. In the following analysis we assume that a medium optically thin is associated to an escape factor equal to 1 whereas for an optically thick medium the escape factor is set to 0.

3.2 SHOCKING

The set of equations of SHOCKING code has been modified to couple the ABBA model with atoms and molecules. Firstly a new set of species conservation equations that includes separate equations for the excited states of the molecules is added to the system (2). Therefore the set of equation to be solved accounts for 116 continuity equations as opposed to 95 continuity equations of the atomic CR model.
Secondly the separate equation for the free-electron energy (see §2) does not include the electronic energy of the molecules but only the electronic energy of atomic ions N^+ and O^+.

3.3 Flowfield results

The analysis starts with the discussion of the temperature and compositions profiles in the post-shock relaxation area. In particular in this section we propose a comparison among the results obtained with the simplified ABBA model described in the first part of this work and the full model described in the present section. Figure (20) shows the evolution of the temperature profiles whose behavior is similar to the results presented in § 1.2.1. As we can observe the new results seems to be closer to the Johnston's results, being the vibrational relaxation slower. Thermal equilibrium is reached only at $2cm$ from the shock front and the vibrational temperatures do not exceed the translational one.

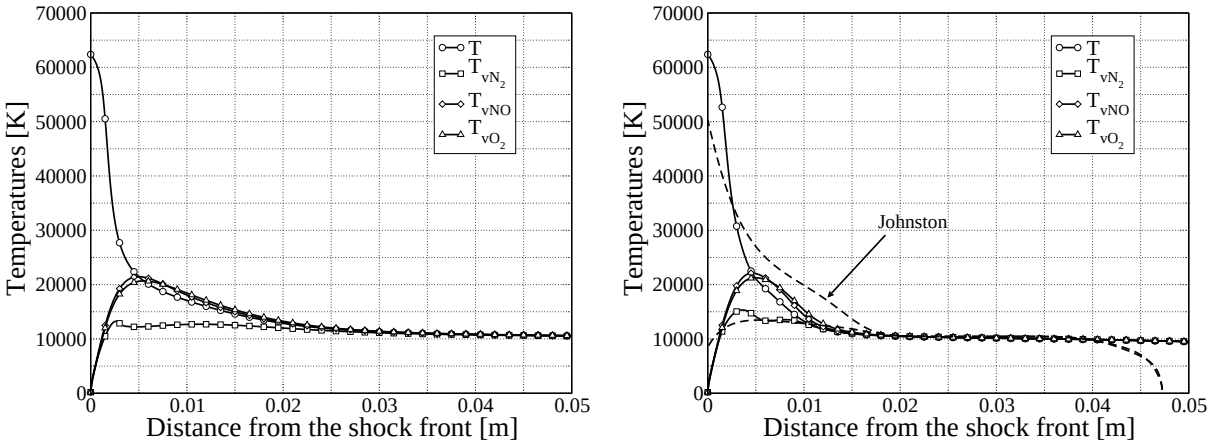

20.1: 20.2:

Figure 20: 1634 s case. (a) Temperature profiles: CR model molecules; (b) Temperature profiles: CR model atoms

Figure (21) compares species evolution in the post shock area. Strong differences are found in the relaxation of the N_2^+. The atomic specific CR model predicts a slow relaxation to the equilibrium values as opposed to the detailed ABBA model which exhibits an overshoot right after the shock. The reason of the disagreement is certainly due to the differences in the kinetic mechanism used for the reaction rate constants. An accurate analysis of the experimental results (28) shows an overshoot in the radiation from the $N_2^+(1-)$ system and suggests a presence of an overshoot in the N_2^+ population consistent with the results given by the more accurate model. A deeper investigation of the problem is required before driving any conclusion however results from literature (37) also confirm the presence of an overshoot in the population of the excited states after the shock.

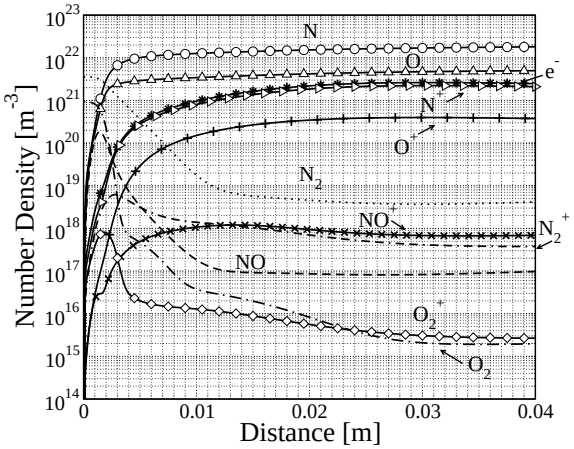

21.1: **CR atoms (part 1)**

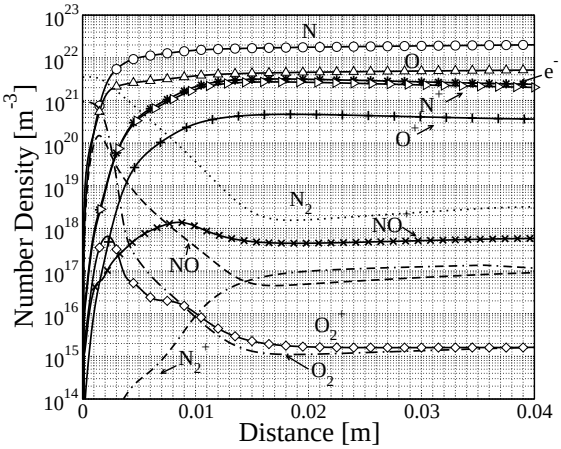

21.2: **CR molecules**

Figure 21: 1634 s case. (a) Population profiles: CR model molecules; (b) Population profiles: CR model atoms

3.4 Results: molecules

Excited states of the molecules are found to be depopulated in the post shock area similarly to the excited states of the atoms. However due to their complicate internal structure (molecules have rotational-vibrational modes) the estimation of the rate constants for the elementary processes governing the detailed kinetics are often unknown or affected by large uncertainty.

N_2^+ Population

The determination of the N_2^+ composition is important since it is a strong radiator in the UV part of the spectrum. Its radiative contribution, due to due to the bound transitions from the N_2^+ ($B^2\Sigma_u^+$) to the N_2^+ ($X^2\Sigma_g^+$), is very important at speed up to $10\,km/s$.
Figure (22.2) shows the population profiles of the ground and the excited states. A strong depopulation of the upper states is shown in figure (22.2) in all the computational domain. Equilibrium conditions are not reached since the medium is considered to be optically thin. As a consequence a reduced emission of the N_2^+1- is to be expected.

The population of the state dictating the intensity of this band system, $B^2\Sigma_u^+$, is governed by the transitions to and from the $A^2\Pi_u$ state below it and the $D^2\Pi_g$ state above it which however is not included into the ABBA model. The $B^2\Sigma_u^+$ can be also formed through a process known as inverse pre-dissociation. There are indeed several repulsive potential passing through the B state potential. One N atom and N^+ approaching along the repulsive potential can transfer into the B state through this process (51). The predissociation can also be a mechanism for draining the B state. The population of the $C^2\Sigma_u^+$ state, from which the Second Negative (2-) system originates, is dictated by the populations in the two free states $N^4S + N^+3P$, $N^2D + N^3P$.

The electron-impact dissociation and heavy-particle impact transitions only contribute noticeably in narrow regions near the shock and the body. Note that this calculation assumes that the molecular radiation is optically thin, which means that the radiation transitions have their maximum possible influence on the depleting process of the B state.

N_2 Population

Figure 22.1 compares the equilibrium population of the N_2 molecules versus the nonequilibrium calculation given by the CR model. The $N_2(A)$ and $N_2(B)$ states, which are closely spaced in energy, are shown to have similar Boltzmann and non-Boltzmann distributions throughout the layer. The $N_2(C)$ state is seen to diverge most from a Boltzmann distribution.

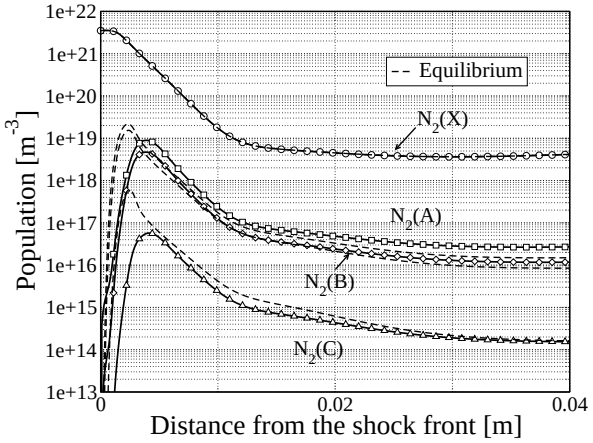

22.1: **Population profiles of N_2 molecules.**

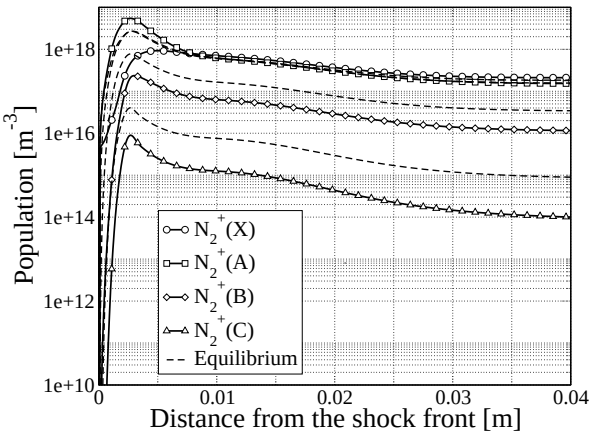

22.2: **Population profiles of N_2^+ molecules.**

Figure 22: 1634 s case. Number density evolution through the shock layer.

NO Population

A comparison of the number densities for NO obtained with the CR model presented here and those obtained with the Boltzmann model are presented in Figure 23 for the Fire II 1634 s case. Large deviations from a Boltzmann distribution is seen to be present for the excited states right after the shock. The CR model predicts a much lower number density, which implies that the radiative emission is reduced proportionately.

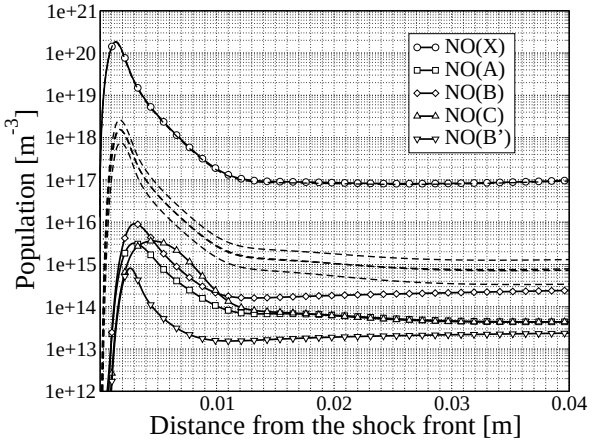

Figure 23: **Population profiles of NO molecules.**

4 Park model: SPRADIAN07

The present section presents a comparison among the ABBA model previously described and the well known SPRADIAN07 code. The nonequilibrium capabilities of the code are used to predict the nonequilibrium population of the excited states of the molecules and atoms.

A new radiation computer code, SPRADIAN07(54; 55; 35) *Structured Package for Radiation Analysis 2007*, is developed jointly by Korea Advanced Institute of Science and Technology and Japan Aerospace Exploration Agency. This code combines and improves on the code NEQAIR85 developed in 1985 and the code SPRADIAN developed in 1999. The code SPRADIAN07 computes both Boltzmann and non-Boltzmann radiations from the given temperatures and species number densities. For radiation under non-Boltzmann excitation, this code solves master equation assuming that a quasi-steady-state (QSS) conditions exists among internal states. In order to carry out such a quasi-steady state calculation, one needs to know the rate coefficients for collisional transitions from all internal states to all other internal states. For atoms, collisional transitions between two electronic states occur mostly by the collisions of electrons. For nitrogen, oxygen, carbon, and hydrogen, which constitute most of the atomic species found in planetary environments that may produce nonequilibrium radiation, electron-impact transition rates are known at least approximately. In the first two parts of the present work, (54; 55) Park compiled the rates of electronic excitation of diatomic molecules, N_2, O_2, NO, CO, CN, and N_2^+ , by electron collisions and by heavy particle collisions needed in the QSS calculation. In Ref.(54), electron-impact transition rates are given in the form of cross sections for bound-bound transitions, and in the form of rate parameters for bound-free transitions. Heavy particle-impact transition rates are given in the form of rate parameters for both bound-bound and bound-free transitions in Ref.(55). Collision partners considered are N, O, N_2, O_2, NO, and CO. The SPRADIAN07 input data files contain these data.

4.1 Results: Comparison with SPRADIAN07

We now present a comparison of our results, in terms of energy distribution of the electronic levels of atoms and molecules with the calculations obtained making use of SPRADIAN07 code.

We start the analysis with the electronic levels of nitrogen atoms. As we can see in figure below (24.1) the Spradian code predicts larger populations for the upper electronic states ($E > 10\,eV$). The population of the ground state and the two metastable states is found to be in Boltzmann equilibrium for the two predictions.
As far as atomic oxygen is concerned Spradian is close to ABBA for low levels. For excited levels, Spradian is closer to equilibrium than ABBA CR.

N_2^+

An accurate comparison in terms of population of excited states among SPRADIAN and ABBA model is shown in figure 25. Both models predict Boltzmann distribution for the ground and the first excited state as opposed to the excited states which are found depleted.

5 Conclusions

In this work, we have studied the departure of the electronic energy populations of molecular and atomic species from Boltzmann distributions for onedimensional air flows obtained in a

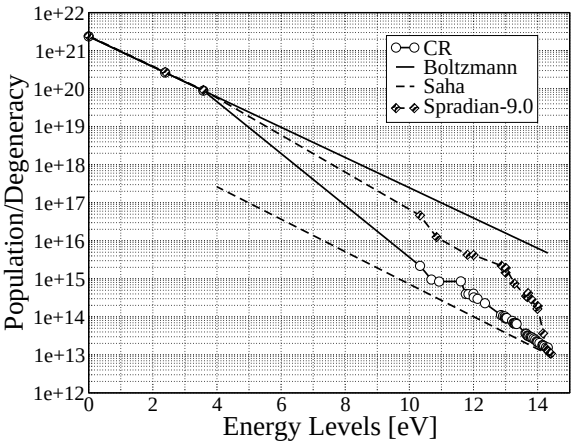

24.1: **Atomic nitrogen.**

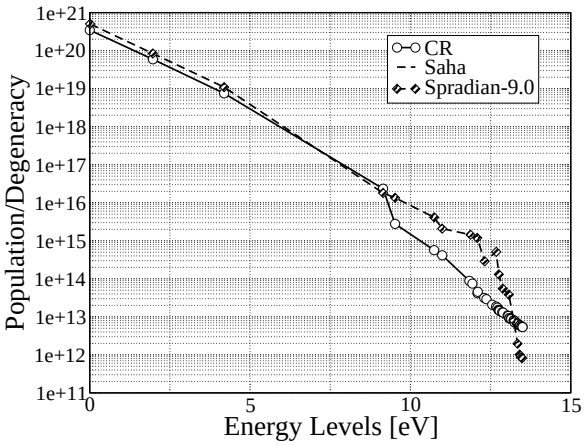

24.2: **Atomic oxygen.**

Figure 24: 1634 s case. Saha diagrams for the excited states of the atomic species.

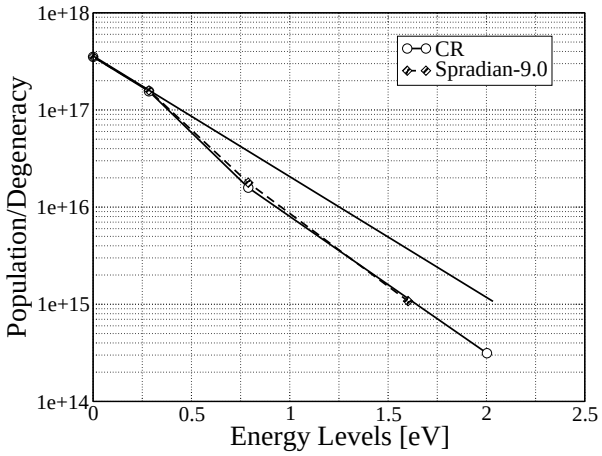

Figure 25: 1634 s case. Saha diagrams for the excited states of N_2^+

shock-tube. The operating conditions are taken from the trajectory of the FIRE II flight experiment and from the test conditions used in the EAST experimental campaign. The results have been obtained by means of a multi-temperature fluid model fully coupled with an electronic-specific collisional radiative model. We have compared the flowfield quantities and electronic energy populations with literature ((34; 37)) and found a good agreement. Moreover a direct comparison of the radiative signature extracted by our 1D solver against the experimental results and have shown good agreement, being all the numerical prediction within 50 % from the experimental value.

The population of the electronic energy levels of the atoms and molecules are found strongly depopulate right after the shock. Deviations from the Boltzmann distribution are found for the upper states that are in equilibrium with the free states. Moreover, the validity of the standard QSS approach widely used by the aerospace community has been tested; the results obtained by means of our full CR model and the standard QSS model are found in good agreement. Metastable states as opposed to the high lying states are found not to respect the QSS assumption this should be accounted for in the future simplified kinetic models by treating them as a separate species in the energy conservation equations. For future high speed reentry application,

one important challenge is related to the necessity to couple the detailed kinetic mechanism of the gas with radiative transfer. The work presented in this report is a first step in this direction.

6 Acknowledgments

Special thanks to my friends Olivier, Thierry, Anne and Arnaud. I would like to acknowledge R. Jaffe, W. Huo, D. Schwanke and G. Chaban for their help their advices and their rates. I would also like to acknowledge S. Moreau, S. Macheret, J. Grinstead and G. Candler for the useful discussions. Special thanks to C. Park and Hyun S. for their radiation code (SPRADIAN07). Least but not last Mickael Playez for his continuous help and support.

References

[1] A.Bourdon, A. Leroux, P. and P.Vervisch (1999). Experiment-modeling comparison in a nonequilibrium supersonic air nozzle flow. *Journal of Thermophysics and Heat Transfer*, 13(1):68–75.

[2] Babou, Y., Rivière, P., Perrin, M. Y., and Soufiani, A. (2007). High-temperature and nonequilibrium partition function and thermodynamic data of diatomic molecules. *International Journal of Thermophysics*.

[3] Babou, Y., Riviere, P., Perrin, M.-Y., and Soufiani, A. (2008). Spectroscopic data for the prediction of radiative transfer in co_2-n_2-o_2 plasmas. *submitted in : Journal of Quantitative Spectroscopy and Radiative Transfer*.

[4] Bose, D. and Candler, G. (1996). Thermal rate constants of the $n2 + ono + o$ reaction using ab initio 3 a and 3 a potential-energy surfaces. *Journal of Chemical Physics*, 104(8):2825.

[5] Bose, D. and Candler, G. (1997). Thermal rate constants of the $o_2 + n \rightarrow no + o$ reaction using ab initio 3 a and 3 a potential-energy surfaces. *Journal of Chemical Physics*, 107(16):6136.

[6] Bose, D., McCorkle, E., and Thompson, C. e. a. (2008). Analysis and model validation of shock layer radiation in air. In *AIAA*, pages AIAA 2008–1246, Reno, Nevada.

[7] Bose, D., Wright, M., Bogdanoff, D., Raiche, G., and Allen, G. A. (2006a). Modeling and experimental assessment of CN radiation behind a strong shock wave. *Journal of Thermophysics and Heat Transfer*, 20:220.

[8] Bose, D., Wright, M. J., Bogdanoff, D. W., Raiche, G. A., and Allen, G. A. (2006b). Modeling and experimental assessement of cn radiation behind a strong shock wave. *Journal of Thermophysics and Heat Transfer*, 20(2):220–230.

[9] Bourdon, A. and Bultel, A. (2006). Detailed and simplified kinetic schemes for high enthalpy air flows and their influence on catalycity studies. *in Experiment, modeling and simulation of gas surface interaction for reactive flows, VKI-LS Rhode-Saint-Genèse, Belgium, February 6-9 2006*, 1:60.

[10] Bourdon, A. and Vervisch, P. (1997). Electron-vibration exchange models in nitrogen flows. *Physical Review E*, 55(4):4634.

[11] Bultel, A., Chéron, B., Bourdon, A., Motapon, O., and Schneider, I. (2006). Collisional-radiative model in air for earth re-entry problems. *Physics of Plasmas*, 13(4):11.

[12] Bultel, A., van Ootegem, B., Bourdon, A., and Vervisch, P. (2002). Influence of ar2 in an argon collisional-radiative model. *Physical Review E*, 65:046406.

[13] Candler, G. V. and MacCormack (1991). Computation of weakly ionized hypersonic flows in thermochemical nonequilibrium. *Journal of Thermophysics and Heat Transfer*, 5(11):266.

[14] Capitelli, M., , Colonna, G., and Armenise, I. (Rhode-Saint-Genèse, Belgium, July 4-7 2002). State-to-state electron and vibrational kinetics in one dimensional nozzle and boundary layer flows. *in Physico-chemical models for high enthalpy and plasma flows*, 1:21.

[15] Capitelli, M., Ferreira, C., Gordiets, B., and Osipov, A. (2000). *Plasma kinetics in Atmospheric Gases*. Springer, Berlin.

[16] Cauchon, D. L. (1967). Radiative heating results from fire ii flight experiment at a reentry velocity of 11.4 km/s. ,Technical Report NASA TM X-1402, Ames Research Center, Moffet Field, Moffet Field.

[17] Chauveau, S., Deron, C., Perrin, M. Y., Riviere, P., and Soufiani, A. (2003). Radiative trasfer in lte air plasmas for temperatures up to 15000 k. *Journal of Quantitative Spectroscopy and Radiative*, 77:113–130.

[18] Chauveau, S., Perrin, M. Y., Riviere, P., and Soufiani, A. (2002a). A contribution of diatomic molecular electronic systems to heated air radiation. *Journal of Quantitative Spectroscopy and Radiative*, 72:503–530.

[19] Chauveau, S. M., Laux, C., Kelley, J. D., and Kruger, C. (2002b). Vibrationally-specific collisional-radiative model for non-equilibrium air plasmas,. *33th AIAA Plasmadynamics and Lasers Conference*. Maui, HW.

[20] Chernyi, G. G.and Losev, S. A., Macheret, S. O., and Potapkin, B. V. (2004). *Physical and Chemical processes in gas dynamics: physical and chemical kinetics and thermodynamics of gases and plasmas*. AIAA, Reston, Virginia.

[21] C.O., L. and C.H., K. (1992). Arrays of radiative transition probabilities for the n_2 first and second positive, *no* beta and gamma, n2 first negative and o2 schumann-runge band systems. *Journal of Quantitative Spectroscopy and Radiative Transfer*. also AIAA paper 1998-2664.

[22] Colonna, G., Capitelli, M., and Giordano, D. (2002). State to state electron and vibrational kinetics in supersonic nozzle air expansion: An improved model. In *AIAA*, pages AIAA 2002–2163, Maui, Hawaii.

[23] Deron, C., Riviere, P., Perrin, M. Y., and Soufiani, A. (2004). Modelling of radiative properties of lte atmospheric plasmas. In *Proceedings of the 15th international conference on gas discharges and their applications*, Toulouse.

[24] Drawin, H. (1963). Atomic cross sections for inelastic collisions. *Report*, pages EUR–CEA–FC 236.

[25] Drawin, H. (1968). Zur formelmssigen darstellung des ionisierungsquerschnitts fr den atom-atomstoss und ber die ionen-elektronen-rekombination im dichten neutralgas. *Zeitschrift fur Physik*, page 404:417.

[26] Dunn, M. G. and Kang, S. W. (1973). Theoretical and experimental studies of reentry plasmas. NASA NTRS CR-2232, NASA.

[27] Frost, R. M., Awakowicz, P., Summers, H. P., and Badnell, N. R. (1998). Calculated cross-sections and measured rate coefficients for electron impact excitation of neutral and singly ionized nitrogen. *Journal of Applied Physics*, 84(6):2989.

[28] Ginstead, J., Wilder, M., Olejniczak, J., D., B., G., A., Dang, K., and Forrest, M. (2008). A comparison of the east shock-tube data with a new air radiation model. In *AIAA*, pages AIAA 2008–1244, Reno, Nevada.

[29] Gnoffo, P. A., Gupta, R. N., and Shinn, J. L. (1989). Conservation equations and physical models for hypersonic air flows in thermal and chemical non-equilibrium. Technical Paper 2867, NASA.

[30] Grinstead, J. H., Olejniczak, J., Wilder, M. C., Bogdanoff, M. W., Allen, G. A., and Lilliar, R. (2007). Shock-heated air radiation measurements at lunar return conditions: Phase i east test report. NASA EG-CAP-07-142.

[31] Gryzinski, M. (1958). Classical theory of electronic and ionic inelastic collisions. *Physical Review*, pages n2–115:374–382.

[Guberman] Guberman, S. Electron-vibration exchange models in nitrogen flows. *Kluwer, Dordrecht.*

[32] Gupta, R. N., Yos, J. M., Thompson, R. A., and Lee, K. P. (1990). A review of reaction rates and thermodynamic and transport properties for an 11-species air model for chemical and thermal non-equilibrium calculations to 30 000 K. Reference Publication 1232, NASA.

[33] Gurvich, L., Veyts, I., and Alcock, C. (1989). Thermodynamic properties of individual substances. *Hemisphere Publishing Corporation*, 1.

[34] Hash, D., Olejniczak, J., Wright, M., Prabhu, D., Pulsonetti, M., Hollis, B., Gnoffo, P., Barnhardt, P., Nompelis, I., and Candler, G. (2007). Fire ii calculations for hypersonic nonequilibrium aerothermodynamics code verification: Dplr, laura,and us3d. In *AIAA*, page 4634, Reno, Nevada.

[35] Hyun, S. Y., Park, C., and Chang, K. S. (2008). Rate parameters for electronic excitation of diatomic molecules, iii. cn radiation behind a shock wave. In *AIAA*, pages AIAA 2008–1276, Reno, Nevada.

[36] Johnston, C. (2008). A comparison of the east shock-tube data with a new air radiation model. In *AIAA*, pages AIAA 2008–1245, Reno, Nevada.

[37] Johnston, C. O. (2006). *Nonequilibrium Shock-Layer Radiative Heating for Earth and Titan Entry.* PhD thesis, Virginia Polytechnic Institute and State University, Virginia.

[38] Knab, O., Frühauf, H., and Messerschmid, E. (1994). Uranus/cvcv model validation by means of thermochemical nonequilibrium nozzle airflow calculations. *Proceeding of the 2nd European Symposium on Aerothermodynamics for Space Vehicles, ESA Publication Div., Noordwijk, The Netherlands*, page 129.

[39] Kossyi, I., Kostinsky, A., Matveyev, A., and Silakov, V. (1992). Kinetic scheme of the non-equilibrium discharge in nitrogen-oxygen mixtures. *Plasma Sources Science and Technology*, (1):207.

[40] Lamet, J. M., Babou, Y., Riviere, P., Perrin, M. Y., and Soufiani, A. (2008). Radiative trasfer in gases under thermal and chemical nonequilibrium conditions: Application to earth atmospheric re-entry. *Journal of Quantitative Spectroscopy and Radiative*, 1:235–244.

[41] Laux, C. O. (Rhode-Saint-Genèse, Belgium, July 4-7 2002). Radiation and nonequilibrium collisional radiative models. *in Physico-chemical models for high enthalpy and plasma flows*, 1:55.

[42] Lee, J. H. (1984). Basic governing equations for the flight regimes of aeroassisted orbital transfer vehicles. Technical Paper 84-1729, AIAA, Snowmass, Colorado.

[43] Lotz, W. (1968). Electron-impact ionization cross sections and ionization rate coefficients for atoms and ions from hydrogen to calcium. *Zeitschrift fur Physik*, page 216(3):241.

[44] Magin, T. E., Caillault, L., Bourdon, A., and Laux, C. O. (2006). Nonequilibrium radiative heat flux modeling for the huygens entry probe. *Journal of Geophysical Research - Planets*, 111:E07S12.

[45] Martin, W. C., Fuhr, J. R., Kelleher, D. R., Masgrove, A., Sugar, J., and Wiese, W. L. (1999). Nist atomic spectra database (version 2.0). *Avaliable from: http://physics.nist.gov/asd2 Gaihersburg.*

[46] Mitchner, M. and Kruger, C. (1973). *Partially ionized gases.* John Wiley and Sons, New York.

[47] Olynick, D., Henline, W. D., Hartung, L., and Candler, G. (1994). Comparisons of coupled radiative navier-stokes flow solutions with the project fire ii flight data. In *AIAA*, pages AIAA 94–1955, Colorado Springs, CO.

[48] Panesi, M., Magin, T., Bourdon, A., Bultel, A., and Chazot, O. (2007). Simulation of nonequilibrium reentry air plasmas by means of a collisional-radiative model. *38th AIAA Plasmadynamics and Lasers Conference.*

[49] Panesi, M., Magin, T., Bourdon, A., Bultel, A., and Chazot, O. (2008). Analysis of the fire ii flight experiment by means of a collisional-radiative model. In *46th AIAA Aerospace Sciences Meeting and Exhibit*, Reno, Nevada.

[Park] Park, C. Problems of rates chemistry in the flight regimes of aeroassisted orbital transfer vehicles. *Thermophysical Aspects of Re-entry Flows edited by J. N. Moss and C. D. Scott AIAA, New York, 1986 , Vol.*

[50] Park, C. (1985). Park, nonequilibrium air radiation (neqair) program : user's manual. ,Technical Report NASA TM86707, Ames Research Center, Moffet Field, Moffet Field.

[51] Park, C. (1989). *Nonequilibrium Hypersonic Aerothermodynamics.* John Wiley and Sons, New York.

[52] Park, C. (1993). Review of chemical-kinetic problems of future nasa mission, I: Earth entries. *Journal of Thermophysics and Heat Transfer*, 7(3):385.

[53] Park, C. (2006). Thermochemical relaxation in shock tunnels. *Journal of Thermophysics and Heat Transfer*, 20(4):689.

[54] Park, C. (2008a). Rate parameters for electonic excitation of diatomic molecules - electon-impact processes. In *AIAA*, pages AIAA 2008–1206, Reno, Nevada.

[55] Park, C. (2008b). Rate parameters for electonic excitation of diatomic moleculesa - heavy particle-impact processes. In *AIAA*, pages AIAA 2008–1206, Reno, Nevada.

[56] Park, C., Jaffe, R., and Partridge, H. (2001). Chemical-kinetic parameters of hyperbolic earth entry. *Journal of Thermophysics and Heat Transfer*, 15(1):76.

[57] Radhakrishnan, K. and Hindmarsh, A. (1993). Description and use of lsode the livermore solver for ordinary differential equations. *NASA reference publication*, 1:124.

[58] Rivière, P. (2002). Systematic semi-classical calulations of stark broadening parameters of ni, oi, nii and oii multiplet for modelling radiative transfer in atmospheric air mixture plasmas. *Journal of Quantitative Spectroscopy and Radiative Transfer*, 73:91–110.

[59] Roberts, T. P. (1996). Implementation into tina modelling for electron-electronic energy equation. In *Thermophysics Conference*, New Orleans, LA.

[60] Sarma, G. S. R. (1958). Physico-chemical modeling in hypersonic flow simulation. *Progress in Aerospace Sciences*, pages 281–349.

[61] Sarrette, J.-P., Gomes A.-M., Bacri, J., Laux, C., and Kruger, C. (2001). Collisional-radiative modeling of quasi-thermal air plasmas with elecronic temperatures between 2000 and 13000 k. *Journal of Quantitative Spectroscopy and Radiative*, 1:53–125.

[62] Scutaru, D., Rosenmann, L., and Taine, J. (1994). Approximate intensities of co2 hot bands at 2.7, 4.3, and 12[mu]m for high temperature and medium resolution applications. 52(6):765–781.

[63] Sharma, S. P. and Park, C. (1990a). Operating characteristics of a 60- and 10-cm electric arc driven shock tube - part i : the driver. *Journal of Thermophysics and Heat Transfer*, 4(3):259–265.

[64] Sharma, S. P. and Park, C. (1990b). Operating characteristics of a 60- and 10-cm electric arc driven shock tube - part ii : the driven. *Journal of Thermophysics and Heat Transfer*, 4(3):266–272.

[65] Surzhikov, S., Rouzaud, O., Soubrie, T., Gorelov, V., and Kireev, A. (2006a). Prediction of non-equilibrium and equilibrium radiation for reentry conditions. In *AIAA*, pages AIAA 2006–1188, Reno, Nevada.

[66] Surzhikov, S., Sharikov, I., Capitelli, M., and Colonna, G. (2006b). Kinetic model of nonequilibrium radiation of strong air shock waves. In *AIAA*, pages AIAA 2006–586, Reno, Nevada.

[67] Team, T. O. P. (1995). The opacity project. *Institute of Physics Publishing, Bristol, Philadelphia*, 1.

[68] Teulet, P., Sarrette, J.-P., and A.-M., G. (1999). Calculation of electron impact inelastic cross sections and rate coefficients for diatomic molecules. *Journal of Quantitative Spectroscopy and Radiative*, 1:69–549.

[69] Teulet, P., Sarrette, J.-P., and A.-M., G. (2001). Collision-radiative modeling of one- and two- temperature air and air-sodium plasmas at atmospheric pressure with temperatures of 2000 - 12000 k. *Journal of Quantitative Spectroscopy and Radiative*, 1:70–159.

[70] Thivet, F. (1992). *Modeling and computation of hypersonic flows in chemical and thermodynamic nonequilibrium (in French)*. PhD thesis, Ecole Cent. Paris, Chatenay-Malabry, France.

Table 1: Index, energy, degeneracy, and secondary quantum number for the N and O electronic energy states considered.

k for N(k)	E_k (eV)	g_k	l_k	k for O(k)	E_k (eV)	g_k	l_k
1	0.000	4	1	1	0.000	9	1
2	2.384	10	1	2	1.970	5	1
3	3.576	6	1	3	4.190	1	1
4	10.332	12	0	4	9.146	5	0
5	10.687	6	0	5	9.521	3	0
6	10.927	12	1	6	10.740	15	1
7	11.603	2	1	7	10.990	9	1
8	11.759	20	1	8	11.838	5	0
9	11.842	12	1	9	11.930	3	0
10	11.996	4	1	10	12.090	25	2
11	12.006	10	1	11	12.100	15	2
12	12.125	6	1	12	12.300	15	1
13	12.357	10	0	13	12.370	9	1
14	12.856	12	0	14	12.550	15	0
15	12.919	6	0	15	12.670	5	0
16	12.972	6	2	16	12.710	3	0
17	12.984	28	2	17	12.740	5	0
18	13.000	26	2	18	12.760	25	2
19	13.020	20	2	19	12.770	15	2
20	13.035	10	2	20	12.780	56	3
21	13.202	2	1	21	12.860	15	1
22	13.245	20	1	22	12.890	9	1
23	13.268	12	1	23	13.030	5	0
24	13.294	10	1	24	13.050	3	0
25	13.322	4	1	25	13.080	40	2
26	13.343	6	1	26	13.087	56	3
27	13.624	12	0	27	13.130	15	1
28	13.648	6	0	28	13.140	9	1
29	13.679	90	2	29	13.220	5	0
30	13.693	126	3	30	13.230	3	0
31	13.717	24	1	31	13.250	168	2
32	13.770	2	1	32	13.330	5	0
33	13.792	38	1	33	13.340	3	0
34	13.824	4	1	34	13.353	96	2
35	13.872	10	1	35	13.412	8	0
36	13.925	6	1	36	13.418	40	2
37	13.969	18	0	37	13.459	8	0
38	13.988	60	2	38	13.464	40	2
39	13.999	126	3	39	13.493	3	0
40	14.054	32	1	40	13.496	40	2
41	14.149	18	0				
42	14.160	90	2				
43	14.164	126	3				
44	14.202	20	1				
45	14.260	108	0				
46	14.316	18	0				

Table 2: Probability $A_{i\to j}$ for $\mathrm{N}(i) \to \mathrm{N}(j<i) + h\nu$ and $\mathrm{O}(i) \to \mathrm{O}(j<i) + h\nu$ spontaneous emission.

i for N(i)	j for N(j)	$A_{i\to j}(s^{-1})$	i for O(i)	j for O(j)	$A_{i\to j}(s^{-1})$
6	1	2.30×10^8	5	1	3.80×10^8
4	1	5.40×10^8	9	1	1.77×10^8
5	2	5.50×10^8	11	1	0.38×10^8
5	3	2.00×10^8	14	1	2.30×10^8
13	2	4.60×10^8	19	1	6.77×10^7
13	3	0.52×10^8	17	2	4.50×10^8
10	6	4.05×10^6	6	4	0.34×10^8
17	2	8.60×10^3	12	4	3.26×10^5
18	2	0.65×10^8	7	5	0.28×10^8
20	2	0.47×10^8	13	5	6.60×10^5
16	3	1.30×10^8	8	6	2.72×10^7
18	3	5.80×10^3	10	6	4.19×10^7
20	3	1.30×10^8	15	6	0.71×10^7
15	2	1.10×10^8	18	6	7.01×10^6
15	3	0.20×10^8	23	6	3.05×10^6
22	6	0.25×10^6	25	6	1.23×10^6
23	6	0.37×10^6	9	7	1.88×10^7
25	6	0.43×10^6	11	7	2.35×10^7
28	2	0.33×10^8	14	7	2.90×10^7
8	4	0.19×10^8	16	7	0.62×10^7
9	4	2.28×10^7	19	7	3.25×10^6
10	4	3.18×10^7	24	7	2.34×10^6
11	5	2.17×10^7	12	8	4.50×10^6
12	5	2.86×10^7	12	10	4.70×10^5
31	5	1.70×10^6			
31	13	1.59×10^7			
22	4	0.02×10^8			
23	4	0.73×10^7			
25	4	0.25×10^7			
21	5	2.34×10^6			
16	7	2.56×10^7			
17	8	3.73×10^7			
19	8	9.92×10^6			
17	9	7.46×10^4			
18	9	6.30×10^6			
19	9	2.48×10^7			
18	10	5.72×10^6			
18	11	1.16×10^7			
20	11	0.06×10^8			
14	8	1.47×10^7			
14	9	0.76×10^7			
27	8	3.89×10^6			
27	9	2.12×10^6			
38	7	2.30×10^5			
37	9	6.10×10^5			

Time [s]	1634	1636	1643
p_1 [Pa]	2.0	5.25	21.3
T_1 [K]	195	210	276
u_1 [m/s]	11 360	11 310	10 480
p_2 [Pa]	3827	9229	24 506
T_2 [K]	62 377	61 884	53 191
u_2 [m/s]	1899	1891	1756

Table 3: Shock-tube flow characteristic quantities.

Table 4: Kinetic models used in the investigation.

	Excitation			Ionization	
Model	Drawin	Gryzinski	Frost	Drawin Ref. (48)	Drawin Ref. (37)
Abba	×			×	
Abba TCNQ	×			×	
Abba Frost			×	×	
Abba Gryzinski		×	×	×	
Abba Modified		×	×		×

Table 5: Operating conditions for the EAST shock-tube experiments considered here (see Ref. (36))

Case	Shock velocity v_s (km.s^{-1})	upstream pressure P (Torr)	acquisition time τ_{acq}
1	10.340	0.3	0.075
2	9.880	0.3	0.98
3	9.165	0.1	0.5
4	9.989	0.1	0.98

Table 6: Species Considered in the present CR model.

Type	Species	State
Molecules	N_2	$X^1\Sigma_g^+$, $A^3\Sigma_u^+$, $B^3\Pi_g$, $C^3\Pi_u$
	O_2	$X^3\Sigma_g^-$, $a^1\Delta_g$, $b^1\Sigma_g^+$, $A^3\Sigma_u^+$,$B^3\Sigma_u^-$
	NO	$X^2\Pi$, $A^2\Sigma^+$, $B^2\Pi$, $C^2\Pi$, $B'^3\Delta$
Molecular ions	N_2^+	$X^2\Sigma_g^+$, $A^2\Pi_u$, $B^2\Sigma_u^+$, $C^2\Sigma_u^+$
	O_2^+	$X^2\Pi_g$, $a^4\Pi_u$, $A^2\Pi_u$,$b^4\Sigma_g^-$
	NO^+	$X^1\Sigma^+$, $a^3\Sigma^+$, $b^3\Pi$, $b'^3\Sigma^-$,$A^1\Pi$